



**SIMULTANEOUS ELECTROCHEMICAL DETECTION OF ASPIRIN, IBUPROFEN  
AND INDOMETHACIN USING COBALT TETRA AMINO PHENOXY  
PHTHALOCYANINE NANOPARTICLES AND NITROGEN DOPED CARBON  
NANODOTS MODIFIED ELECTRODE**

**BY**

**NYARADZAI DONDO**

**R142795A**

Submitted in partial fulfillment of the requirements for the degree of

**Bachelor of Science Honours in Chemical Technology**

**Department of Chemical Technology**

in the

**Faculty of Science and Technology**

at the

**Midlands State University, Gweru, Zimbabwe**

**Supervisors: Prof. M. Moyo**

**Dr. M. Shumba**

## **DEDICATION**

The research is dedicated to my late parents who laid the foundation of my destiny and my relatives who stood by me against all odds during the course of this degree.

## **ACKNOWLEDGEMENTS**

My profound gratitude goes to my supervisors Dr M. Shumba and Prof M. Moyo for their continuous encouragement, invaluable advice, guidance and insight throughout this research. I am also greatly indebted to Samson Matema for his extensive support throughout my studies, may God bless you abundantly. Sincere gratitude also goes to Dondo family and fellow friends for their unwavering support. I would like to thank the MSU Chemical Technology laboratory staff for their contributions in making the research possible. Finally, I would like extend my gratitude to the Almighty God for all the blessings he granted for me.

## ABSTRACT

Carbon nanodots (CNDs), nitrogen doped carbon nanodots (n-CNDs) and their composites with cobalt tetra aminophenoxy phthalocyanine nanoparticles (CoTAPhPcNPs) were employed towards the simultaneous detection of aspirin (ASA), ibuprofen (IBU) and indomethacin (INDO). The nanomaterials were characterized by FTIR, UV-Vis, TEM, cyclic voltammetry, electrochemical impedance spectroscopy, linear sweep voltammetry, chronoamperometry and differential pulse voltammetry. CoTAPhPcNPs/n-CNDs-GCE showed excellent electrooxidation of ASA, IBU and INDO and oxidation overpotentials were lowered. Higher surface coverages were observed indicating that modifiers were lying flat on the surface of the electrode. The CoTAPhPcNPs/n-CNDs-GCE gave catalytic rate constants of  $1.655 \times 10^1 \text{ M}^{-1}\text{s}^{-1}$ ,  $1.42 \times 10^1 \text{ M}^{-1}\text{s}^{-1}$  and  $1.91 \text{ M}^{-1}\text{s}^{-1}$  for ASA, IBU and INDO respectively. The detection limits observed for ASA, IBU and INDO were  $9.66 \times 10^{-7}$ ,  $4.19 \times 10^{-7}$  and  $7.2 \times 10^{-7} \text{ M}$  respectively. The adsorption equilibrium constants for ASA, IBU and INDO were found to be  $1.05 \times 10^5 \text{ M}^{-1}$ ,  $1.2 \times 10^5 \text{ M}^{-1}$  and  $5.56 \times 10^5 \text{ M}^{-1}$  respectively. Furthermore, high Tafel slopes were observed indicating adsorption of each analyte to the surface of the electrode. The Gibb's free energy for ASA, IBU and INDO were found to be  $-28.63 \text{ kJ mol}^{-1}$ ,  $-28.96 \text{ kJ mol}^{-1}$  and  $-27.07 \text{ kJ mol}^{-1}$  respectively. The developed sensor exhibited an excellent anti-interference property and good reproducibility towards the detection of ASA, IBU and INDO.

**DECLARATION**

I, Nyaradzai Dondo R142795A, hereby declare that I am the sole author of this dissertation. I authorize Midlands State University to lend this dissertation to other institutions or individuals for the purpose of scholarly research.

Signature .....

Date .....

## APPROVAL

This dissertation entitled “*Simultaneous electrochemical detection of aspirin, ibuprofen and indomethacin using cobalt tetra aminophenoxy phthalocyanine nanoparticles and nitrogen doped carbon nanodots modified electrode*” by Nyaradzai Dondo meets the regulations governing the award of the degree of Chemical Technology of Midlands State University, and is approved for its contribution to knowledge and literal presentation.

Supervisor.....

Date.....

## LIST OF ABBREVIATIONS

**CNDs**-Carbon nanodots

**n-CNDs**- Nitrogen doped carbon nanodots

**CoTAPhPcNPs**- Cobalt tetra aminophenoxy phthalocyanine nanoparticles

**CoTAPhPcNPs/CNDs**- Cobalt tetra aminophenoxy phthalocyanine nanoparticles/carbon nanodots

**CoTAPhPcNPs/n-CNDs**- Cobalt tetra aminophenoxy phthalocyanine nanoparticles/nitrogen doped carbon nanodots

**ASA**- Aspirin

**IBU**- Ibuprofen

**INDO**-Indomethacin

**MPcs**-Metallophthalocyanines

**DPV**- Differential pulse voltammetry

**EIS**- Electrochemical impedance spectroscopy

**GCE**- Glassy carbon electrode

**LOD**- Limit of detection

**LOQ**- Limit of quantification

**UV-Vis**- Ultraviolet visible spectroscopy

**FTIR**- Fourier Transform Infrared

## TABLE OF CONTENTS

DEDICATION.....	i
ACKNOWLEDGEMENTS.....	ii
ABSTRACT .....	iii
DECLARATION .....	iv
APPROVAL .....	v
LIST OF ABBREVIATIONS.....	vi
TABLE OF CONTENTS .....	vii
LIST OF FIGURES .....	xi
LIST OF TABLES .....	xiii
<b>CHAPTER ONE .....</b>	<b>1</b>
1.0 Introduction.....	1
1.1 Background.....	1
1.2 Aim of the study.....	2
1.3 Objectives .....	2
1.4 Problem statement.....	3
1.5 Justification.....	3
<b>CHAPTER TWO .....</b>	<b>5</b>
<b>LITERATURE REVIEW .....</b>	<b>5</b>
2.1 Carbon nanodots and synthesis.....	5
2.1.1 Electrochemical synthesis.....	6
2.1.2 Microwave/ultrasonic synthesis.....	6
2.1.3 Arc discharge.....	7
2.1.4 Laser ablation/passivation.....	7

2.1.5 Heterogeneous CNDs .....	7
2.2 Phthalocyanines .....	8
2.2.1 Discovery .....	8
2.2.2 Tetrapyrrole Macrocycles .....	8
2.2.3 Nomenclature of Pcs and Numbering of the benzene carbons on Pcs .....	10
2.2.4 Synthesis of Phthalocyanines.....	10
2.2.5 Synthesis of Phthalocyanines used in this work .....	11
2.2.6 Synthesis of Phthalocyanine nanoparticles .....	12
2.2.7 Applications of CNDs and Phthalocyanines .....	13
<b>CHAPTER THREE .....</b>	<b>14</b>
<b>METHODOLOGY.....</b>	<b>14</b>
3.0 Introduction.....	14
3.1 Reagents and chemicals.....	14
3.2 Equipment.....	15
3.3 Synthesis procedures .....	15
3.3.1 Synthesis of carbon nanodots.....	15
3.3.2 Synthesis of nitrogen doped carbon nanodots .....	16
3.3.3 Synthesis of Cobalt (II) tetra aminophenoxy phthalocyanine (CoTAPhPc) .....	16
3.3.4 Synthesis of Cobalt tetra aminophenoxy phthalocyanine nanoparticles (CoTAPhPcNPs)....	16
3.4 Physical characterization of synthesized products.....	17
3.5 Electrode modification .....	17
3.6 Electrochemical characterization .....	18
3.6.1 Electrochemical behavior of modified electrodes.....	18
3.6.2 Electrochemical Impedance Spectroscopy .....	19
3.7 Optimization of pH.....	19

3.8 Electrocatalytic Detection of Analytes .....	20
3.9 Order of reaction .....	21
3.10 Determination of Gibbs energy .....	21
3.11 Catalytic rate constant .....	21
3.11.1 Limit of Detection using DPV .....	22
3.12 Effect of concentration using Impediometric technique.....	22
3.13 Simultaneous Detection .....	22
3.14 Stability Studies .....	22
3.15 Reproducibility.....	23
3.16 Applicability .....	23
3.17 Effect of interference .....	23
<b>CHAPTER FOUR.....</b>	<b>24</b>
4.1 FTIR characterization.....	24
4.2 UV-vis characterization.....	25
4.3 TEM characterization .....	26
4.4 Electrochemical Characterization .....	27
4.4.1 Cyclic Voltammetry. ....	27
4.4.2 Nyquist plots .....	29
4.4.3 Bode Plots .....	31
4.5 Surface Coverage .....	32
4.6 Electrocatalytic detection of the Drugs .....	33
4.6.1 pH optimization.....	33
4.6.2 Electrocatalytic Detection of ASA, IBU and INDO .....	35

4.6.3 Electrochemical Impedance Spectroscopic studies of aspirin, Ibuprofen and indomethacin .....	36
4.6.4 Bode plots .....	38
4.6.5 Simultaneous Cyclic Voltametry Studies .....	39
4.6.6 Kinetic Studies .....	40
4.6.7 Tafel Slopes .....	42
4.6.8 Order of Reaction .....	43
4.6.9 Determination of Gibbs' energy.....	44
4.6.10 Determination of Catalytic Rate Constant .....	47
4.6.11 Determination of Limit of Detection .....	48
4.6.12 Simultaneous Differential Pulse Voltametry Studies .....	51
4.6.13 Effect of concentration using Impediometric Technique .....	54
4.6.14 Stability Studies.....	54
4.6.15 Reproducibility Studies .....	55
4.6.16 Applicability.....	56
4.6.17 Interference Studies .....	58
<b>CHAPTER FIVE.....</b>	<b>60</b>
5.1 Conclusion .....	60
5.2 Recommendations .....	61
References .....	62
APPENDIX .....	629

## LIST OF FIGURES

Fig 2.1: schematic diagram of electrochemical fabrication of CNDs .....	6
Fig 2.2: structures of macrocycles; pyrrole unit, unsubstituted porphyrine, porphyrazine, MPc, H2Pc, and NPc .....	9
Fig 2.3: Notation and naming of Pcs .....	10
Fig 2.4: Scheme for the synthesis of the CoTAPhPc .....	11
Fig 2.5: schematic presentation of immobilization Metallophthalocyanines .....	12
Fig 4.1: FTIR spectra of the electrode modifiers. ....	24
Fig 4.2: UVVIS spectra for (i) CNDs (ii) n-CNDs (iii) CoTAPhPcNPs .....	26
Fig 4.3: (A) TEM image of CNDs and (B) diameter distribution of the CNDs .....	27
Fig 4.4: (A) CVs in 1mM Ferri/Ferro in 0.1M KCl, (a) CNDs-GCE, (b) n- CNDs-GCE, (c) Bare-GCE, (d) CoTAPhPcNPs-GCE (e) CoTAPhPcNPs/CNDs-GCE (f) CoTAPhPcNPs/n-CNDs-GCE (B) Nyquist plots in 1mM Ferri/Ferro in 0.1M KCl, (C) Bode plots in 1mM Ferri/Ferro in 0.1M KCl .....	28
Fig 4.4B shows Nyquist plots obtained for the modified electrodes .....	29
Fig 4.5: Cyclic voltammograms of the modified electrodes in pH 6 phosphate buffer solution. Scan rate 100mV/s .....	33
Fig 4.6: Optimization of Ph for each analyte in PBS. Scan rate 100mV/s.....	34
Fig 4.7: CVs, Nyquist plots and Bode plots for ASA, IBU and INDO, (a) CoTAPhPcNPs-GCE, (b) CoTAPhPcNPs/CNDs-GCE, (c) ) CoTAPhPcNPs/n-CNDs-GCE .....	38
Fig 4.8: Simultaneous Cyclic voltammograms responses in 1mM ASA/IBU, 1mM ASA/INDO, 1mMIBU/INDO, 1mM ASA/IBU/INDO in PBS. ....	40
Fig 4.9: Effect of scan rate on peak potentials and currents a) 50mV/s b) 100 mV/s, c) 150 mV/s, d) 200 mV/s, e) 250 mV/s, f) 300 mV/s, g) 350 mV/s, h) 400 mV/s on CoTAPhPcNPs/n-CNDs-GCE for ASA, IBU and INDO oxidation. [ ] = 1mM. Inset: plot of $I_{pa}$ vs $\sqrt{v}$ . ....	41
Fig 4.10: Plot of potential versus log scan rate in 1mM (A) ASA, (B) IBU and (C) INDO.....	43

Fig 4.11: Cyclic voltammograms for (a) 5 mM , (b) 10mM, (c) 15mM (d) 20mM and (e) 25mM of ASA (pH 4), IBU (pH 5) and INDO (pH 6) concentrations in PBS. Inset plot of log $I_{pa}$ vs log [ASA, IBU, INDO] .....	44
Fig 4.12: Linear sweep voltammograms and Langmuir adsorption isotherm plot for CoTAPhPcNPs/n-CNDs-GCE (10 $\mu$ M, 20 $\mu$ M, 30 $\mu$ M, 40 $\mu$ M, 50 $\mu$ M, 60 $\mu$ M) of ASA, IBU and INDO concentrations in PBS. ....	45
Fig 4.13: Chronoamperograms (Insert-dependence concentration on current) and plots of $I_{cat}/I_{buff}$ versus $t^{1/2}$ (10-60 $\mu$ M) in PBS determined using chronoamperometry for CoTAPhPcNPs/n-CNDs-GCE.....	46
Fig 4.14: DPV for CoTAPhPcNPs/n-CNDs-GCE in: a) 0.1 $\mu$ M, b) 0.2 $\mu$ M, c) 0.3 $\mu$ M, d) 0.4 $\mu$ M, e) 0.5 $\mu$ M, f) 0.6 $\mu$ M ASA, IBU and INDO Inset: Plot of $I_{pa}$ vs [ASA, IBU, and INDO] ..	50
Fig 4.15: DPV for CoTAPhPcNPs/n-CNDs-GCE in PBS (ph 5.5) containing a mixture of A: 0.2-1.2 $\mu$ M INDO, 0.2 $\mu$ M IBU. B: 0.2-1.2 $\mu$ M IBU, 0.2 $\mu$ M INDO. Insets show the relationship of $I_{pa}$ versus the concentrations of each analyte.....	53
Fig 4.16: Complex plane impedance spectra at CoTAPhPcNPs/n-CNDs-GCE for different concentrations of IBU in ph 5 PBS and variation of $R_{ct}$ with log [IBU] .....	54
Fig 4.17: Continuous cyclic voltammetric evolutions for (A) ASA, (B) IBU and (C) INDO in PBS at CoTAPhPcNPs/n-CNDs-GCE.Scan rate = 100 mV/s.....	55
Fig 4.18: Cyclic voltammograms of (A) ASA, (B) IBU and (C) INDO in PBS at CoTAPhPcNPs/n-CNDs-GCE.....	56
Fig 4.19: DPVs of the real sample analysis for each analyte .....	57
Fig 4.20: DPVs for (A) (i) ascorbic acid and (ii) ASA (B) (i) citric acid and (ii) IBU and (C) (i) glucose and (ii) INDO in PBS at n-CNDs/CoTAPhPcNPs GCE.....	59

## LIST OF TABLES

Table 2.1: Functions of CNDs and conjugated CNDs .....	13
Table 3.1: working electrodes used in this research .....	18
Table 3.2: Parameters in cyclic voltametry .....	19
Table 3.3: Parameters for ph studies in 1 mmol aspirin, 1 mmol ibuprofen and 1 mmol indomethacin.....	20
Table 4.1: Electrochemical parameters for the modified electrodes.....	30
Table 4.2: Electrochemical parameters of the modified electrodes for each analyte .....	36
Table 4.3: Summary of the chronoamperometry studies .....	48
Table 4.4: Detection limits of ASA, IBU and INDO.....	51
Table 4.5: Determination of drugs in waste water effluent using CoTAPhPcNPs/n-CNDs-GCE	58

## CHAPTER ONE

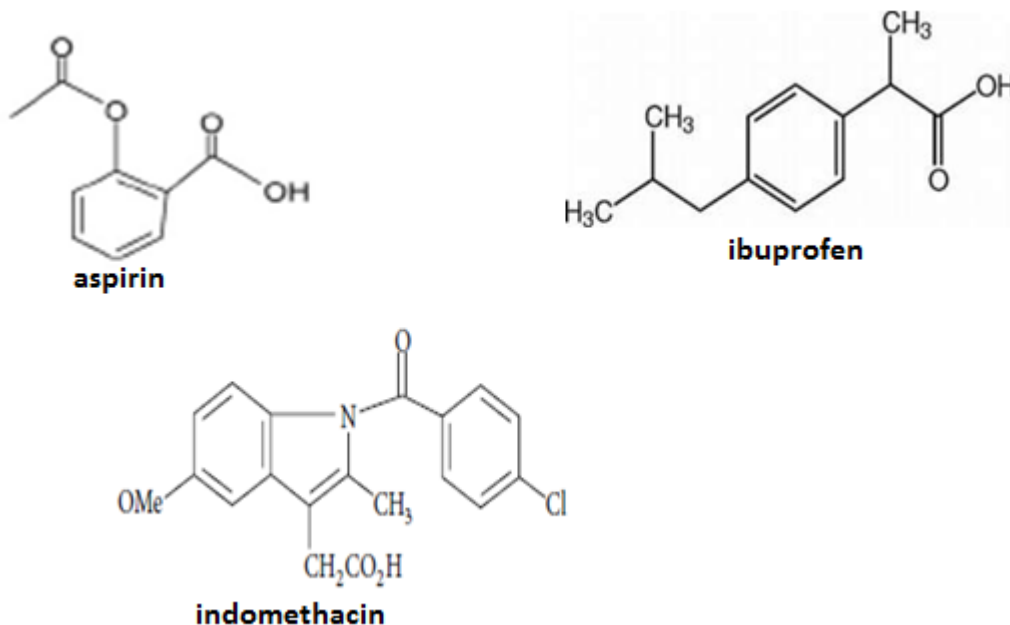
### 1.0 Introduction

The chapter gives an overview of the research aims, objectives, problem statement and justification on the electro detection of aspirin, ibuprofen and indomethacin using nitrogen doped carbon nanodots and cobalt tetra amino phenoxy phthalocyanine nanoparticles.

### 1.1 Background

The non-steroidal anti-inflammatory drugs consisting of aspirin (ASA), ibuprofen (IBU) and indomethacin (INDO) are used to reduce hormones that cause inflammation and to treat pain from conditions such as headache, muscle aches, menstrual cramps, arthritis, backache, fever and primary dysmenorrhea [1]. However, an overdose of these drugs may induce nausea, vomiting, diarrhea, abdominal pain, sweating, seizures, confusion or an irregular heartbeat. Hence, their determination in trace quantities is of great importance [2]. Previously, electrochemical techniques have been implemented for the estimation of IBU, ASA and INDO when present individually. The most common techniques for the determination of ASA, IBU and INDO in commercial dosage form were based on ratio spectra [3], capillary zone electrophoresis [4], chromatography [5], UV-vis spectrophotometry [6], . Moreover, these methods face the drawbacks of being expensive, laborious and requiring pretreatment of the samples, are solvent usage intensive, require expensive devices and maintenance[2]. Surprisingly, no voltammetric procedure exists for the simultaneous determination of ASA, IBU and INDO in a mixture. Therefore, it is desirable to develop simple, sensitive and precise alternate methods employing a modified glassy carbon electrode for the simultaneous determination of aspirin, ibuprofen and indomethacin. Chemically modified electrodes are used to lower the detection limits compared to

bare electrodes. Pristine carbon nanodots (CNDs), nitrogen doped carbon nanodots (n-CNDs) and phthalocyanine have triggered a new genre for the development of novel electrode materials due to their amazing structural, mechanical, electrical and physical properties.



## 1.2 Aim of the study

To assess the efficiency of the modified glassy carbon electrode using nitrogen doped nanodots and cobalt tetra amino phenoxy phthalocyanine nanoparticles on the electrochemical detection of aspirin, ibuprofen and indomethacin.

## 1.3 Objectives

- To synthesize carbon nanodots (CNDs), nitrogen doped carbon nanodots (n-CNDs) and cobalt tetra amino phenoxy phthalocyanine nanoparticles (CoTAPhPcNPs)
- To characterize the electrode modifiers using FTIR, Uv-vis and TEM
- To determine the optimum pH and reaction kinetics during detection of ASA, IBU and INDO at CoTAPhPcNPs/n-CNDs-GCE electrode surface.

- To detect ASA, IBU and INDO at a) CoTAPhPcNPs GCE , b) CoTAPhPcNPs/CNDs-GCE c) CoTAPhPcNPs/n-CNDs-GCE.
- To perform simultaneous detection of ASA/IBU, ASA/INDO, IBU/INDO and ASAI/IBU/INDO by employing cyclic voltammetry and differential pulse voltammetry technique.
- To perform reproducibility, stability and applicability studies of the developed electrode towards oxidation of ASA, IBU and INDO.

#### **1.4 Problem statement**

The non-steroidal anti-inflammatory drugs such as aspirin, ibuprofen and indomethacin can cause serious or fatal adverse effects when taken in overdose. Higher dose of ASA, IBU and INDO causes negative side effects in humans. For these reasons, it is important to analyze these drugs in real samples [2]. The widespread use of these drugs and the need for clinical and pharmacological study require fast and sensitive analytical techniques to determine the presence of aspirin, ibuprofen and indomethacin in pharmaceutical formulations.

#### **1.5 Justification**

Due to instrumental problems, there is a need to develop a modified electrode that is able to detect aspirin, ibuprofen and indomethacin at very low concentrations, affordable cost, efficient and selective determination. Some of the clinical methods are time consuming hence electrochemical methods based on chemically modified electrodes have attracted much attention because of quick response, high sensitivity and selectivity in the determination of trace level analytes. Voltammetric techniques particularly cyclic voltammetry (CV), chronoamperometry

and differential pulse voltammetry (DPV) are employed as alternative methods for the detection and electrochemical behavior of aspirin, ibuprofen and indomethacin [7]. Research into the development of electrochemical sensors continues to be rapidly growing in electrochemistry. Improvements in the selectivity, stability and scope of such sensors are highly desirable in order to meet challenges posed by clinical samples. Therefore in the present study carbon nanodots, nitrogen doped carbon nanodots and MPcs are used as they have good electron transfer properties. Chemically linking them could produce very good electron transfer mediators for electrocatalysis. It has been observed that nanosized MPc molecules have good electrocatalytic properties than their bulk counterparts hence our choice in this study [8]. Co is chosen to be the central metal due to the well-known electrocatalytic activity of CoPc derivatives. Aminophenoxy substituent was also chosen due to the bulky nature which prevent aggregation [9]. Carbon nanodots were used in this study because of their chemical inertness, low toxicity and ease of functionalization [10]. The modifiers were used together in order to reduce the over potential of the glassy carbon electrode and also to increase sensitivity towards the simultaneous detection of ASA, IBU and INDO.

## CHAPTER TWO

### LITERATURE REVIEW

The section gives an outline of carbon nanodots (CNDs), nitrogen doped carbon nanodots, phthalocyanines and their applications.

#### 2.1 Carbon nanodots and synthesis

Carbon nanodots (CNDs) are a new class of carbon nanomaterials with sizes below 10 nm. The first CNDs were obtained by during purification of single-walled carbon nanotubes through preparative electrophoresis in 2004. CNDs have become a rising star in the nanocarbon family and this is due to their abundant, benign and inexpensive nature [11]. CNDs have been introduced to semiconductor materials including CNDs/TiO<sub>2</sub> and CNDs/Fe<sub>3</sub>O<sub>4</sub> due to their excellent electron transfer ability [12]. The exciting property of CNDs is their photoluminescence, which can be tuned by varying the excitation wavelength. Moreover, CNDs show low toxicity and they can be synthesized from an unlimited number of carbon sources, with feasible large scale production and excellent chemical – and – stability [10]. Nuclear magnetic resonance measurements showed that carbon atoms of CNDs that are derived from candle soot were sp<sup>2</sup> hybridized with no saturated sp<sup>3</sup> carbon atoms and this indicates that CNDs are conjugated systems. CNDs are most superior in terms of high aqueous solubility, inexpensive [13], robust chemical inertness, easy functionalization, outstanding photoluminescent properties [14], low toxicity and excellent biocompatibility [15]. By introducing the synthesis, structure and properties of CNDs in this study, the goal is to provide further insight to stimulate further research on the potential applications of CNDs, such as in photocatalysis, bioimaging, optoelectronics and sensors [11]. The amphoteric charge transfer character of CNDs emerged as

a focal point as it has been intensively investigated in non-covalent electron donor–acceptor hybrids [16]. The current methods that have been used for synthesizing CNDs are classified into two groups: top-down and bottom-up. Top-down methods include laser ablation, electrochemical oxidation, electrochemical soaking. The bottom-up methods that build up CNDs from small molecules include microwave irradiation and thermal oxidation [17].

### 2.1.1 Electrochemical synthesis

Electrochemical synthesis of CNDs was achieved when they grew multiwalled carbon nanotubes (MWCNTs) from scrolled graphene layers on carbon paper by chemical vapor deposition (CVD). CNDs are produced electrochemically by oxidizing a graphitic column electrode against a saturated calomel electrode with a Pt wire counter electrode in  $\text{NaH}_2\text{O}_4$  aqueous solution [11].

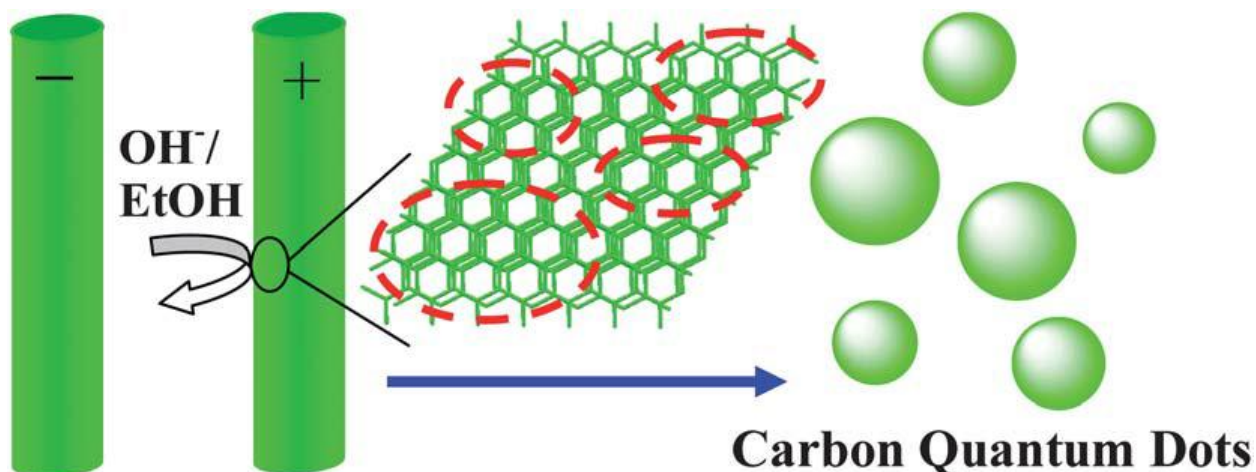


Fig 2.1: schematic diagram of electrochemical fabrication of CNDs [11]

### 2.1.2 Microwave/ultrasonic synthesis.

Microwave or ultrasonic technology has become a very important process in synthesis of CNDs. In this method, different amounts of polyethylene glycol 200 (PEG200) and saccharide were

added to distilled water to form a transparent solution. The solution was then heated in a 500 W microwave oven for some minutes. When the reaction time was increased, the solution changed from colorless to yellow, and a dark brown color was finally produced, which implied the formation of CNDs [11].

### **2.1.3 Arc discharge.**

The arc soot is oxidized with 3.3 M HNO<sub>3</sub> to introduce carboxyl functional groups, and then extracted the sediment with NaOH solution (pH 8.4) to produce a stable black suspension. The suspension was then separated by gel electrophoresis into short tubular carbons, SWCNTs and a very fast moving band of highly fluorescent material, which was composed of CNDs [11].

### **2.1.4 Laser ablation/passivation.**

CNDs can also be produced via laser ablation of a carbon target in the presence of water vapor with argon as a carrier gas at 900 °C and 75 kPa. After refluxing in HNO<sub>3</sub> for up to 12h and surface passivation by combining simple organic species such as poly(propionylethyleneimine-co-ethyleneimine (PPEI-EI)), the acid-treated CNDs will then give bright luminescence emission. By selecting good organic solvents, the surface states of CNDs could then be modified to achieve tunable light emission. Majoring on control experiments, the origin of the luminescence was attributed to the surface states related to the ligands on the surface of CNDs [11].

### **2.1.5 Heterogeneous CNDs**

CNDs can be doped with other elements such as nitrogen, phosphorus and boron to widen their applications. Doping CNDs can improve chemical bonding, electronegativity and also a lone pair

of electrons from either nitrogen or phosphorus can be readily transferred to p-orbitals of  $sp^2$  carbon structures and also better electronic properties can be achieved [18].

## **2.2 Phthalocyanines**

### **2.2.1 Discovery**

Phthalocyanines (Pcs) were discovered in 1907 [19] and they were used as dyes given their characteristic blue–green color [20]. The central cavity of Pcs is known to be capable of accommodating 63 different elemental ions, including hydrogen (metal-free phthalocyanine,  $H_2$ -Pc). The time frame between 1930 and 1950 allows the full elucidation of the Pc chemical structure to be determined and the properties of the Pcs were also investigated. As a result of these studies, it was observed that Pcs are highly colored, planar 18  $\pi$ -electron aromatic ring systems similar to porphyrins [19]. Pcs form complexes by substitution of the two weakly acidic hydrogen atoms at inner nitrogen sites by divalent positively charged coordination centers [21].

### **2.2.2 Tetrapyrrole Macrocycles**

Pcs are classified to be macrocyclic compounds since they are bivalent, tetradentate, planar, 18  $\pi$ -conjugated electron aromatic ring systems. Pcs are composed of four pyrrole units that are linked by four aza ( $—N=C—$ ) groups at the  $\alpha$ -carbon of pyrrole unit and they have four aza bridges and four phenylene rings [19].

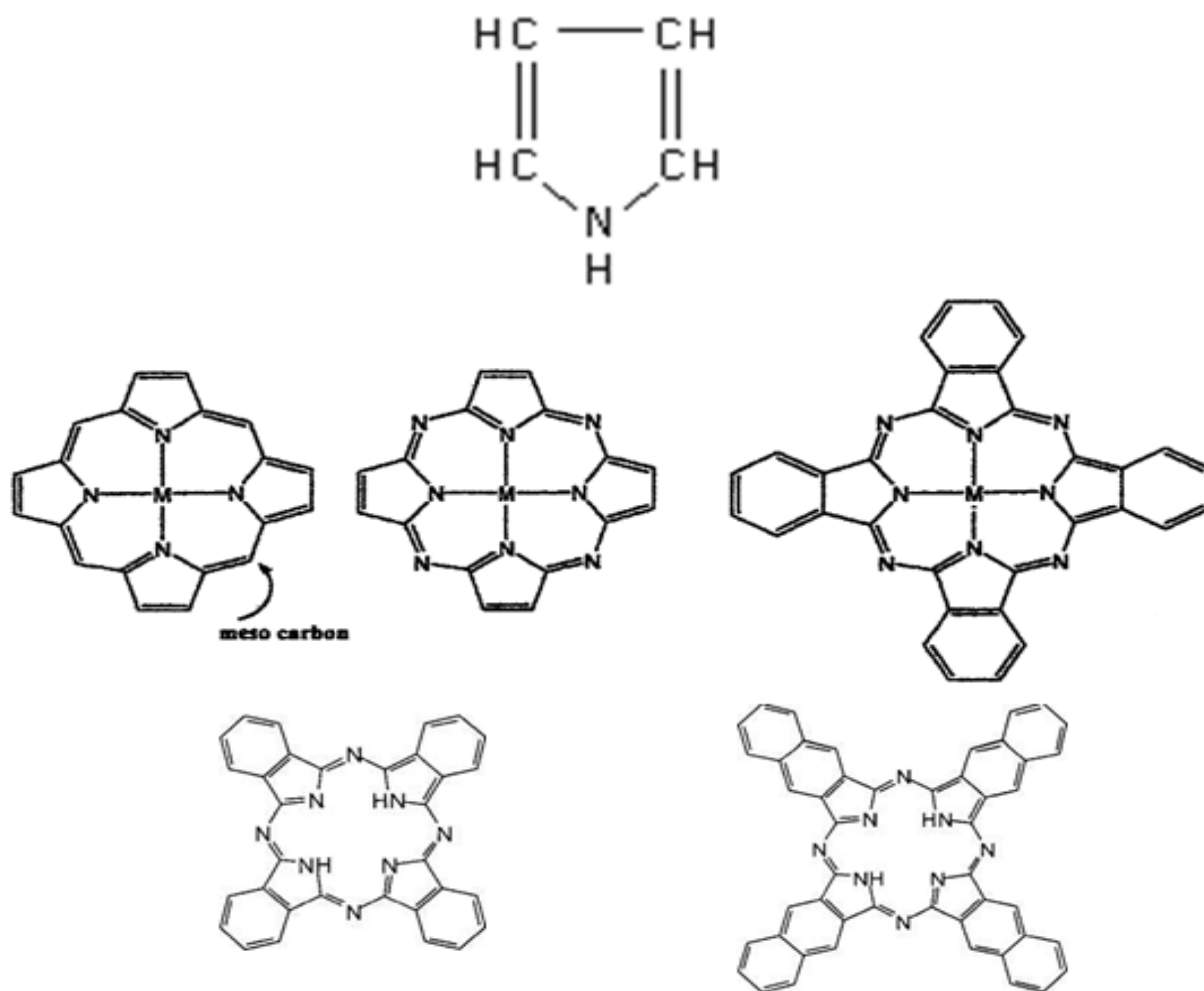


Fig 2.2: structures of macrocycles; pyrrole unit, unsubstituted porphyrine, porphyrazine, MPc, H<sub>2</sub>Pc, and NPc [19]

### 2.2.3 Nomenclature of Pcs and numbering of the benzene carbons on Pcs

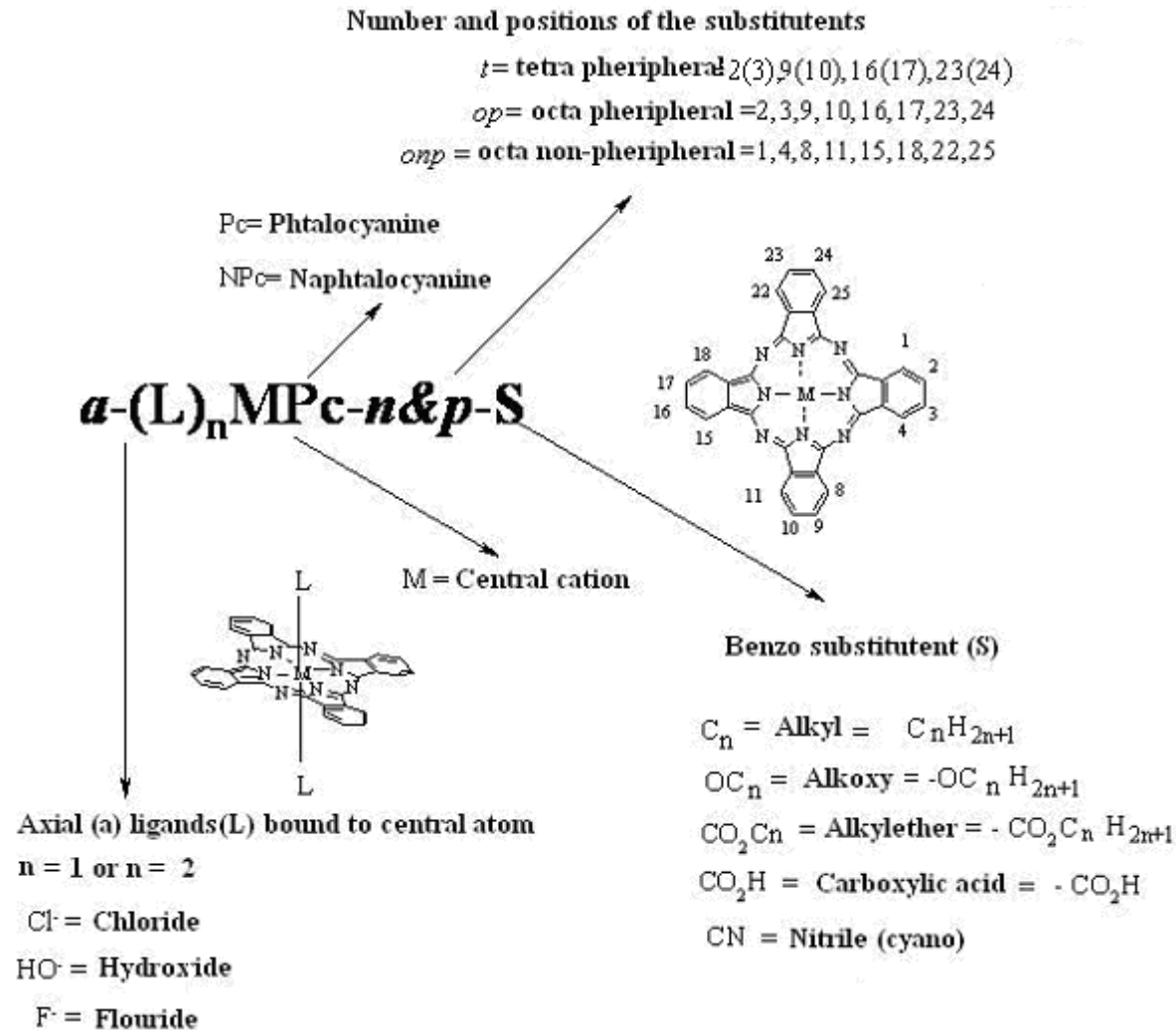


Fig 2.3: Notation and naming of Pcs [19]

### 2.2.4 Synthesis of phthalocyanines

Various 1,2-disubstituted benzene precursors have been used successfully for phthalocyanine synthesis that is phthalonitriles, isoindolines, phthalic acid, phthalimides, phthalic acid and anhydride derivatives, 1,2- dibromobenzenes and cyanobenzamide. Depending on the base,

temperature, solvent, nature of the substituents, type of precursor, metal salt and the metal that has to be inserted into the macrocycle with wide range of conditions have been utilised.

### 2.2.5 Synthesis of phthalocyanines used in this work

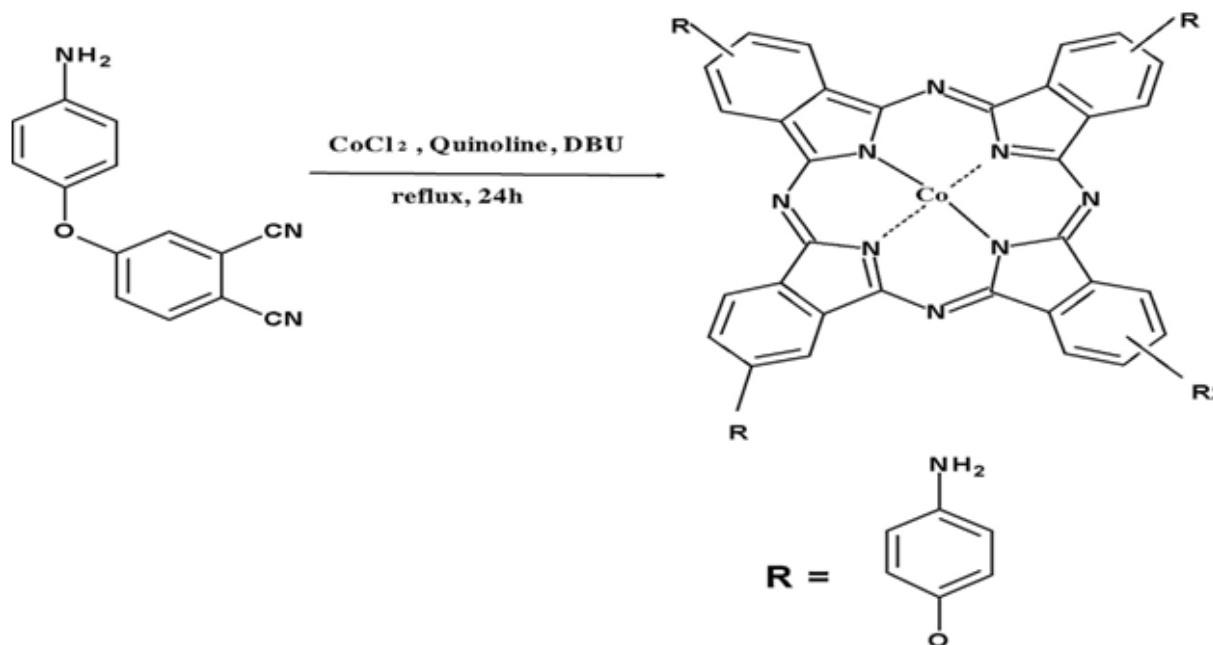


Fig 2.4: Scheme for the synthesis of the CoTAPhPc [9]

In this work, a mass of 300 mg of 4-amino-phenoxy phthalonitrile was mixed with 42 mg of anhydrous cobalt chloride. A volume of 3 ml of quinoline was added to the mixture. The mixture was refluxed for 24 h. The product was cooled to room temperature. It was washed several times with methanol, ethanol, hexane, water and diethyl ether successively. The residue was dried and then subjected to Soxhlet extraction in ethanol/water ratio 1:1 solvent mixture for seven days. The product was oven dried at 80 °C for 48 h [9].

## 2.2.6 Synthesis of phthalocyanine nanoparticles

Nanosized MPC molecules have shown better electrocatalytic properties than their bulk counterparts. Cobalt was chosen as the central metal due to its electrocatalytic activity of CoPc derivatives. Aminophenoxy substituent was used due to the bulky nature which can prevent aggregation [9]. In this work, cobalt tetra amino phenoxy phthalocyanine nanoparticles were prepared as described elsewhere for other MPC complexes [8]. Briefly, a mass of 0.15 mg of CoTAPhPc was dissolved in 5 ml of sulphuric acid (98%). The solution was added drop wise to a vigorously stirring 300 ml aqueous solution of hexadecyltrimethyl ammonium bromide. The resulting solution was washed successively with water until the water was at pH 7. The solid residue was dried at 80<sup>0</sup>C in an oven for 24 h. The resulting nanoparticles were dispersed in dry DMF by sonication for 1h. Many approaches have been employed to immobilize MPCs and these are physical adsorption onto support surface, encapsulation within porous materials, electrostatic interaction between oppositely charged complexes and surface, grafting via direct coordination of metal to support, and covalent anchoring to support [22].

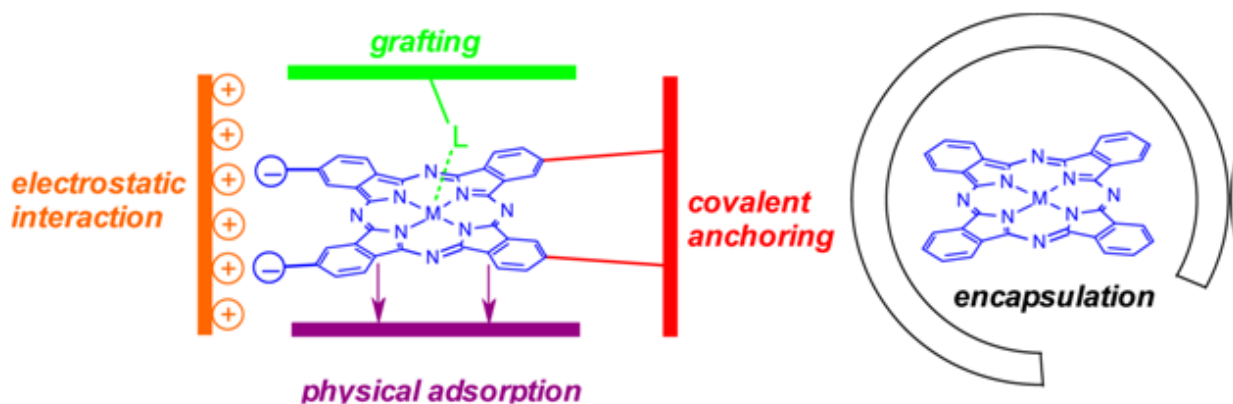


Fig 2.5: schematic presentation of immobilization Metallophthalocyanines

### 2.2.7 Applications of CNDs and phthalocyanines

CNDs have been utilized in many fields such as bioimaging, biosensing, electrocatalysis, super capacitors and solar cells. Functions of the phthalocyanine include photosensitization, photovoltaic light absorption, conductivity, electronic sensors, synthetic metals and optoelectronics.

Table 2.1: Functions of CNDs and conjugated CNDs

Nanomaterial	Mode of Detection	Analyte	Reference
CQDs-Pt@Bi <sub>2</sub> WO <sub>6</sub> /FTO	Electrocatalysis	methanol	[12]
C-dots/ZrO <sub>2</sub>	Electrocatalysis	methyl parathion	[23]
N-CNDs	Fluorescence	Nitrite	[24]
N-CNDs	Fluorescence	Silver ions	[25]
N-doped C-dots	Colorimetric and Ratiometric Fluorescence	Iodide ions	[26]
CDs based dual-emission silica nanoparticles	Ratiometric Fluorescence	Vanadium (V)	[27]
Nitrogen doped carbon	Electrocatalysis	Caffeic acid	[28]
Poly (o-aminophenol) and graphene quantum dots	Electrocatalysis	Levofloxacin	[29]
Carbon nanodots	Electrocatalysis	Ferric ions	[30]
CoTAPhPcNPs/n-CNDs	Electrocatalysis	ASA,IBU,INDO	This work
CoTAPhPcNPs/n-CNDs	Electrocatalysis	ASA,IBU,INDO	This work

## CHAPTER THREE

### METHODOLOGY

#### 3.0 Introduction

The chapter is an outline of chemicals, equipment, synthetic routes and characterization techniques used in this study. Electrochemical behavior of the CoTAPhPcNPs/n-CNDs towards the detection of ASA, IBU and INDO was evaluated using cyclic voltammetry, electrochemical impedance spectroscopy (EIS), chronoamperometry, linear sweep voltammetry and differential pulse voltammetry (DPV). Factors such as adsorption isotherms, pH and scan rate were investigated to evaluate the applicability of the best electrode in the detection of ASA, IBU and INDO.

#### 3.1 Reagents and chemicals.

Chemicals used in this study were of pure analytical grade and used directly without further purification unless stated. Potassium ferrocyanide ( $K_4[Fe(CN)_6]$ ) (Associated Chemical Enterprise) sodium hydroxide (NaOH) (ACE), dimethylformamide (DMF) (ACE), ethanol ( $C_2H_5OH$ ) (Glassworld), potassium chloride (KCl) (ACE), hydrochloric acid (HCl) (ACE), ascorbic acid ( $C_6H_8O_6$ ) (ACE), melamine (ACE), potassium ferricyanide ( $K_3[Fe(CN)_6]$ ) (ACE), di-sodium hydrogen orthophosphate ( $Na_2HPO_4$ ) (ACE), sodium di-hydrogen orthophosphate ( $NaH_2PO_4$ ) (ACE), ibuprofen, indomethacin, diethyl ether (ACE), de-ionized water (MSU Laboratory), salicylic acid (Skylabs), dichloromethane (Glassworld), methanol (ACE), hexane (Glassworld), cobalt chloride (ACE), potassium bromide (ACE).

## **3.2 Equipment**

All the electrochemical experimental procedures were carried out using Autolab Potentiostat PGSTAT302F installed a 1.10 version NOVA software employing a convectional three electrode system. The three electrode system constituted of a bare glassy carbon electrode which was the working electrode, a platinum wire which was working as an auxiliary/counter electrode and Ag/AgCl (3.0 M) which was working as the reference electrode. All the experiments that were conducted in the study were carried out at room temperature conditions 25 °C. A digital analytical balance (model JJ224BC) was used for weighing. The pH studies of the solutions were adjusted by a Thermoscientific Orion Star A211 pH meter. FTIR spectra were obtained using Thermoscientific Model equipped with OMNIC software. Sonicator model KQ-250B was used for agitation of samples.

## **3.3 Synthesis procedures**

### **3.3.1 Synthesis of carbon nanodots**

CNDs were prepared as described before [31]. Briefly, a mass of 1.1 g of ascorbic acid was weighed and dissolved in 25 ml de-ionized water and 25 ml ethanol (95%) to form a homogeneous solution. Then 25 ml as prepared solution was transferred into autoclave and heated at 180 °C for 4 h. The solution was cooled to room temperature naturally. The dark brown solution was extracted with dichloromethane. The solution was heated in oven for 24 h to obtain a solid mixture of CNDs.

### **3.3.2 Synthesis of nitrogen doped carbon nanodots**

A mass of 2 g of CNDs was weighed and mixed together with 10 g melamine. The mixture was ground using pestle and mortar to form a homogeneous mixture. The mixture was placed in the crucible for 20 mins. The mixture was then heated to 500 °C where the temperature was maintained for 30 mins. Heating was then continued to 1000 °C and the temperature was maintained for 30 mins. The muffle furnace was allowed to cool to room temperature and nitrogen doped CNDs were obtained [32].

### **3.3.3 Synthesis of cobalt (II) tetra aminophenoxy phthalocyanine (CoTAPhPc)**

A mass of 300 mg of 4-amino-phenoxy phthalonitrile was mixed with 42 mg of anhydrous cobalt chloride. A volume of 3 ml of quinoline was added to the mixture. The mixture was refluxed for 24 h. The product was cooled to room temperature. It was washed several times with methanol, ethanol, hexane, water and diethyl ether successively. The residue was dried and then subjected to Soxhlet extraction in ethanol/water ratio 1:1 solvent mixture for seven days. The product was oven dried at 80 °C for 48 h [9].

### **3.3.4 Synthesis of cobalt tetra aminophenoxy phthalocyanine nanoparticles (CoTAPhPcNPs)**

Cobalt tetra amino phenoxy phthalocyanine nanoparticles were prepared as described elsewhere for other MPc complexes [8]. Briefly, a mass of 0.15 mg of CoTAPhPc was dissolved in 5 ml of sulphuric acid (98%). The solution was added drop wise to a vigorously stirring 300 ml aqueous solution of hexadecyltrimethyl ammonium bromide. The resulting solution was washed successively with water until the water was at pH 7. The solid residue was dried at 80 °C in an oven for 24 h. The resulting nanoparticles were dispersed in dry DMF by sonication for 1h.

### **3.4 Physical characterization of synthesized products**

#### **FTIR characterization**

All the synthesized products CNDs, n-CNDs, CoTAPhPcNPs, CNDs/ CoTAPhPcNPs and n-CNDs/ CoTAPhPcNPs were characterized by FTIR spectrophotometer model. A mass of 0.01 g of samples were mixed with 1 g KBr in pestle and mortar to form a pellet and this was characterized within the range 400-4000  $\text{cm}^{-1}$ .

#### **3.5 Electrode modification**

The glassy carbon electrode (GCE) was polished on Buehler Felt pad using Alumina (<10  $\mu\text{m}$ ) and then was ultrasonically cleaned in ethanol for about 10 min. The electrode was further cleaned in water for about 10 min. The electrode was finally rinsed with distilled water and then air dried. The cleaned glassy carbon electrode was modified using drop and dry method. Modifiers used were CNDs, n-CNDs and CoTAPhPcNPs (table 3.1). CoTAPhPcNPs were placed on top of carbon based materials. An aliquot (0.5  $\mu\text{L}$ ) of each modifier was placed on the polished GCE, dried in an oven at 70  $^{\circ}\text{C}$  before use [9]. The electrodes are designated as CNDs-GCE, n-CNDs-GCE, CoTAPhPcNPs-GCE. For the addition of CoTAPhPcNPs on CNDs-GCE and n-CNDs-GCE, 0.5 ml of 1 mg/ml of CoTAPhPcNPs was added on top of CNDs-GCE or n-CNDs-GCE surface followed by drying. The electrodes are represented as CoTAPhPcNPs/CNDs-GCE and CoTAPhPcNPs/n-CNDs-GCE (Table 3.1).

Table 3.1: working electrodes used in this research

Electrode modifier	Method of modification	Electrode designation
Bare glass carbon electrode	-	BGCE
Carbon nanodots	Drop and dry	CNDs GCE
Nitrogen doped carbon nanodots	Drop and dry	n-CNDs GCE
Cobalt tetra aminophenoxy phthalocyanine nanoparticles	Drop and dry	CoTAPhPcNPs GCE
Cobalt tetra aminophenoxy phthalocyanine nanoparticles/Carbon nanodots	Drop and dry	CoTAPhPcNPs/CNDs- GCE
Cobalt tetra aminophenoxy phthalocyanine nanoparticles/Nitrogen doped carbon nanodots	Drop and dry	CoTAPhPcNPs/n-CNDs-GCE

### 3.6 Electrochemical characterization

#### 3.6.1 Electrochemical behavior of modified electrodes

Cyclic voltammetry was used for investigation of electron transfer kinetics for the bare GCE, CNDs-GCE, n-CNDs-GCE, CoTAPhPcNPs-GCE, CoTAPhPcNPs/CNDs-GCE and CoTAPhPcNPs/n-CNDs-GCE. The study was carried out in 1 mM  $[\text{FeCN}_6]^{3-/4-}$  solution at a scan rate of 100 mV/s from -0.4 to 0.6 V (table 3.2, for other parameters).

Table 3.2: Parameters in cyclic voltametry

Start potential (V)	-0.600
Upper vertex potential (V)	0.200
Lower vertex potential (V)	-0.600
Stop potential (V)	-0.600
Step potential	0.00244
Scan rate (mV/s)	100

### 3.6.2 Electrochemical impedance spectroscopy

Nyquist plots and bode plots were performed using Electrochemical Impedance Spectroscopy in 1 mM  $[\text{FeCN}_6]^{3-/4-}$  solution for all electrodes in order to confirm resistance and charge transfer emanating from structural differences of the modifiers compared to results obtained in cyclic voltametry.

### 3.7 Optimization of pH

The effect of pH was studied in the range from pH 4 to 8. The buffer solution was adjusted using 0.1 M NaOH and 0.1 M HCl. The studies were carried out by preparing different pH phosphate buffer solution containing 1 mmol ASA, IBU or INDO. Parameters used are in table 3.3

Table 3.3: Parameters for ph studies in 1 mM aspirin, 1 mM ibuprofen and 1 mM indomethacin.

	Aspirin	Ibuprofen	Indomethacin
Start potential (V)	0.0	0.0	0.0
Upper vertex potential (V)	1.00	1.500	1.500
Lower vertex potential (V)	0.0	0.0	0.0
Stop potential (V)	0.0	0.0	0.0
Scan rate (V/s)	0.100	0.100	0.100

### 3.8 Electrocatalytic detection of analytes

Comparative studies were performed in phosphate buffer solution containing 1 mM ASA, 1 mM IBU OR 1 mM INDO. The studies were carried out using modified electrodes CoTAPhPcNPs-GCE, CoTAPhPcNPs/CNDs-GCE and CoTAPhPcNPs/n-CNDs-GCE in order to confirm increase in anodic peak currents on the oxidation of each analyte. Scan rate studies of each analyte were carried out in order to determine reaction kinetics. The studies were done using CoTAPhPcNPs/n-CNDs-GCE. Cyclic voltametry was used for this study. Parameters used were similar to those in table 3.3 but using different scan rates from 0.50 to 0.400 V/s. This study was performed in order to determine whether the detection of each analyte was diffusion controlled or not. This was observed on plotting graphs of anodic peak current against square root of scan rate.

### 3.9 Order of reaction

This was carried out by varying concentrations of each analyte independently and cyclic voltammetry was used. The range was from 5 mM - 25 mM. The behavior was observed on CoTAPhPcNPs/n-CNDs-GCE at 0.1 V/s scan rate and potential range from 0.0 to 1.5 V. The order of reaction was obtained by plotting the graph of log current against log concentration of each analyte.

### 3.10 Determination of Gibbs energy

The study was conducted using working standard solutions of each analyte 10  $\mu\text{M}$ , 20  $\mu\text{M}$ , 30  $\mu\text{M}$ , 40  $\mu\text{M}$ , 50  $\mu\text{M}$  and 60  $\mu\text{M}$ . The response behavior was observed on CoTAPhPcNPs/n-CNDs-GCE by using linear sweep voltammetry and plots were obtained after keeping the electrode in a stirred solution for 20 min (to allow adsorption). Langmuir adsorption theory was applied (equation 3.1) to give a plot of the ratio of each analyte to catalytic current against concentration of each analyte [9].

$$\frac{[Analyte]}{I_{cat}} = \frac{1}{\beta I_{max}} + \frac{[Analyte]}{I_{cat}} \quad (3.1)$$

Gibbs free energy change due to adsorption  $\Delta G^{\circ}$  was calculated using equation 3.2

$$\Delta G^{\circ} = -RT \ln \beta \quad (3.2)$$

### 3.11 Catalytic rate constant

Chronoamperometry was used to perform catalytic studies. The studies were performed by preparing working standard solutions 10  $\mu\text{M}$ , 20  $\mu\text{M}$ , 30  $\mu\text{M}$ , 40  $\mu\text{M}$ , 50  $\mu\text{M}$  and 60  $\mu\text{M}$  from 1mm stock solution of each analyte. The prepared working standard solutions were filled in the electrochemical cell respectively and the behavior was observed on CoTAPhPcNPs/n-CNDs-GCE. Catalytic rate constant was obtained by plotting graph of slope against square root of

analyte concentration. The gradient of the slope is equivalent to  $\pi k$  which gives the catalytic rate constant.

### **3.11.1 Limit of detection using DPV**

The study was carried out by preparing working standard solution of 0.1  $\mu\text{M}$ , 0.2  $\mu\text{M}$ , 0.3  $\mu\text{M}$ , 0.4  $\mu\text{M}$ , 0.5  $\mu\text{M}$  and 0.6  $\mu\text{M}$  from 1mM stock solution of each analyte. The behavior was observed on CoTAPhPcNPs/n-CNDs-GCE. The limit of detection of each analyte was calculated using  $3\sigma/s$  where  $\sigma$  is the standard deviation of the intercept of buffer solution and  $s$  is the slope of the calibration curve. The limit of quantitation for each analyte was calculated using  $10\sigma/s$ .

### **3.12 Effect of concentration using Impediometric technique**

The study was carried out by preparing working standards solutions of 0.2  $\mu\text{M}$ , 0.4  $\mu\text{M}$ , 0.6  $\mu\text{M}$ , 0.8  $\mu\text{M}$ , 1  $\mu\text{M}$  and 1.2  $\mu\text{M}$  of IBU. The behavior was observed at CoTAPhPcNPs/n-CNDs-GCE by using electrochemical impedance spectroscopy.

### **3.13 Simultaneous detection**

Differential pulse voltammetry possesses higher sensitivity than cyclic voltammetry technique so it was further utilized to evaluate the performance of the CoTAPhPcNPs/n-CNDs-GCE for the analysis of IBU and INDO. The working standards solutions were prepared for each analyte

### **3.14 Stability studies**

Stability studies were performed using the CoTAPhPcNPs/n-CNDs-GCE for each analyte by performing 20 cycles by using cyclic voltammetry at 0.1 V/s scan rate at a potential 0.0 to 1.5V.

### **3.15 Reproducibility**

The developed sensor was analyzed for each analyte by employing the cyclic voltametry technique. Before and after each analysis, the electrode was dipped in distilled water and sonicated for five minutes in order to remove adhered particles at the surface of electrode. The scan rate was at 0.1 V/s and potential was from 0.0 to 1.5 V.

### **3.16 Applicability**

The study was carried out by employing the DPV technique. The developed sensor was used to detect each analyte in waste water. The waste water was spiked with aliquots amount of each analyte.

### **3.17 Effect of interference**

Differential pulse voltametry was used to investigate the interference for each analyte. Equimolar solutions of analytes were prepared in the same matrix with phosphate buffer solution. The mixture was analyzed from 0 to 1.5 V.

## CHAPTER FOUR

This chapter presents results obtained during the research.

### 4.1 FTIR characterization

FTIR was performed to study the nature of the functional groups attached to surface of modifier.

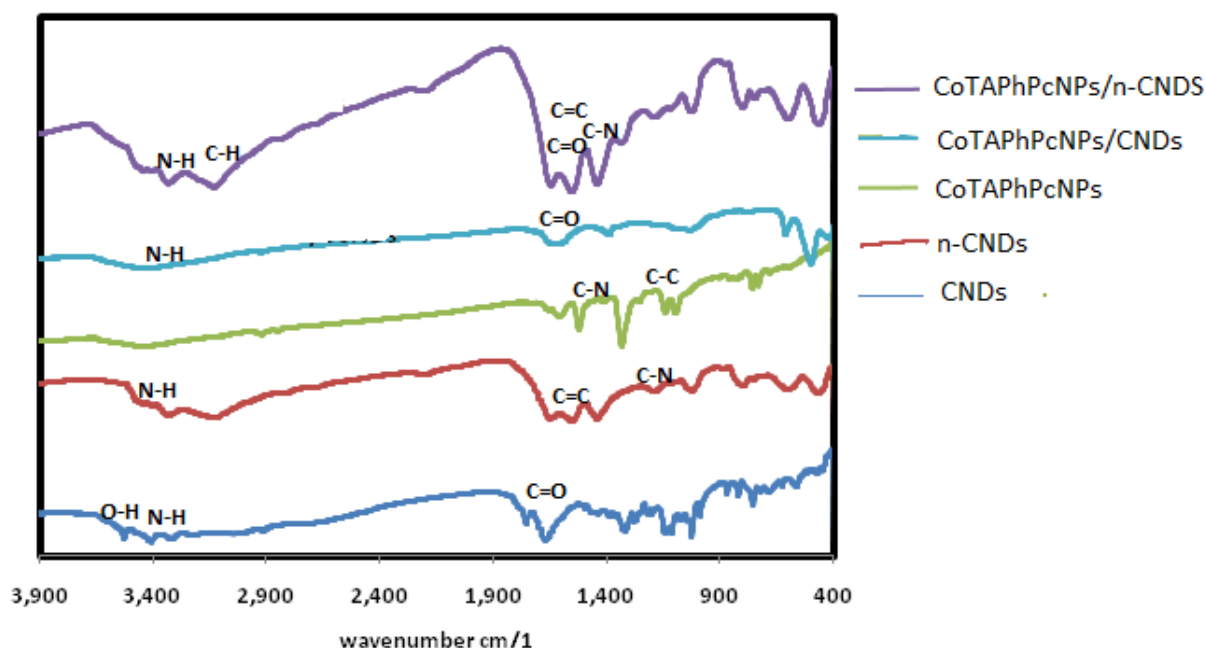


Fig 4.1: FTIR spectra of the electrode modifiers.

The peak at  $1672\text{ cm}^{-1}$  in Figure 4.1 can be attributed to C=O stretching vibration in CNDs. CNDs consist of various functional groups like COOH, OH and N-H. The observed groups were similar to those found in literature [33]. The characteristic absorption band of N-H ( $3424\text{ cm}^{-1}$ ) and the aromatic C-N heterocycles stretching vibrations at  $1420\text{ cm}^{-1}$  can be observed in fig 4.1 for n-CNDs. Moreover, there is a good signal of aromatic C=C stretching at  $1624\text{ cm}^{-1}$  to  $1685\text{ cm}^{-1}$  and this indicates the presence of an  $sp^2$  hybridized honeycomb lattice. Therefore, the prepared n-CNDs exhibit the distinctive  $sp^2$  graphite structure and the observed functional groups are much similar to those reported in literature [18]. The nitrogen doped carbon nanodots

with various oxygen and nitrogen related groups consist of carbonyl, carboxyl, amide, ether and C-O groups. An FTIR spectrum for CoTAPhPcNPs was studied in Figure 4.1. The Ar-O-Ar and aromatic C-C and C-N stretching were observed at 1175-1288  $\text{cm}^{-1}$  and 1574-1288  $\text{cm}^{-1}$  respectively. The absence of C-N triple bond of the starting material at 2230  $\text{cm}^{-1}$  in the spectra confirmed the formation of CoTAPhPcNPs upon their tetramerization reactions. Aromatic C-H stretching vibration of the compound was observed around 3244  $\text{cm}^{-1}$ . An FTIR spectrum for CoTAPhPcNPs/CNDs was also studied in Figure 4.1. The N-H stretching of amino groups were observed. The peak at 1672  $\text{cm}^{-1}$  can be attributed to C=O stretching vibration. Functional groups like COOH, OH and N-H for CoTAPhPcNPs/CNDs were present. The C-N triple bond disappeared in the spectra confirming the formation of for CoTAPhPcNPs/CNDs. An FTIR spectrum for CoTAPhPcNPs/n-CNDs was observed in Figure 4.1. The CoTAPhPcNPs/n-CNDs showed that they have various oxygen and nitrogen related groups consist of carbonyl, carboxyl, amide and C-O groups. The C-N triple bond disappeared in the spectra confirming the formation of CoTAPhPcNPs/n-CNDs.

#### **4.2 UV-Vis characterization**

The optical characteristics of CNDs were studied by UV-vis. Figure 4.2A, depicts the uv-vis spectra of CNDs where one peak is observed and the peak is observed at 340 nm and this corresponds to the n to anti pi transition of C=O bond. Figure 4.2B shows the uv-vis spectra for n-CNDs. The broad peak observed at 320nm is associated with the n to anti pi transition of C=O. Figure 4.2C shows the characteristic bands observed for CoTAPhPcNPs. The Q band for CoTAPhPcNPs is observed at 680nm and vibronic band at 620nm. The broadness of Q band is a typical of amino substituted phthalocyanines [34]. The band is also assigned to the pi to anti pi transition from the highest occupied molecular orbital to the lowest unoccupied molecular orbital

of the phthalocyanine ring. On the other hand, the absorption band at peak 320nm in the UV region is attributed to the transitions from deeper pi levels to the lowest unoccupied molecular orbital.

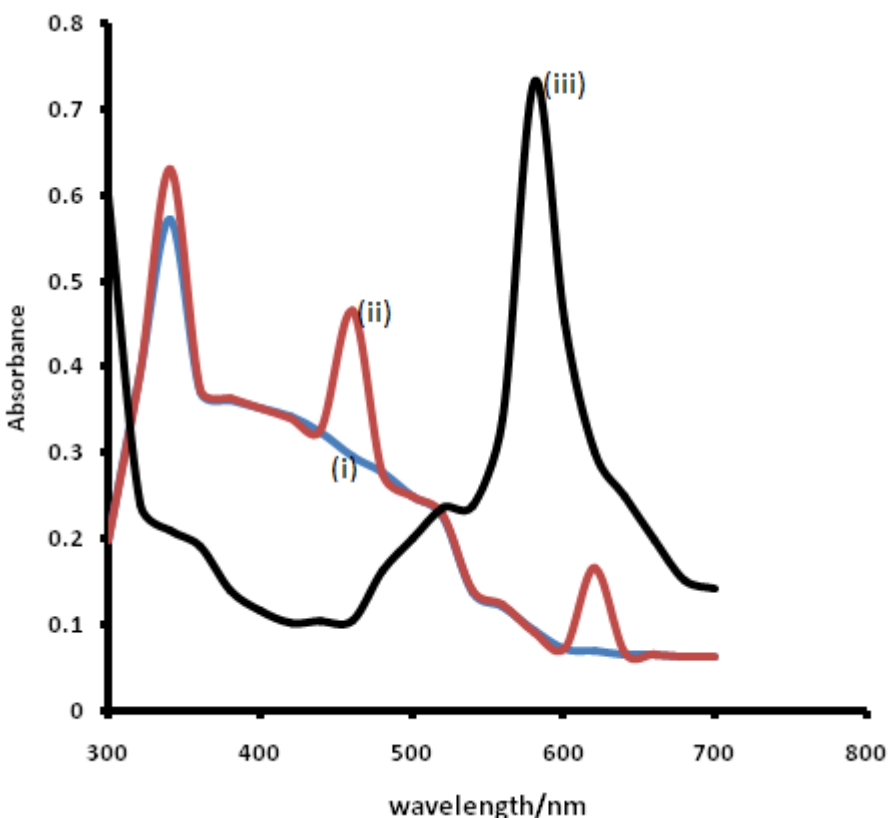


Fig 4.2: UVVIS spectra for (i) CNDs (ii) n-CNDs (iii) CoTAPhPcNPs

### 4.3 TEM characterization

TEM image of the synthesized CNDs is shown in Figure 4.3A. The quasi-spherical morphology was revealed for the synthesized CNDs [35]. The synthesized CNDs in Figure 4.3A consist of irregular and thick shapes forming large aggregations. Oval like structures [36] were also observed in Figure 4.3A. Particle size calculated from TEM image was in the range of 40-130 as shown in fig 4.3B. The average diameter was found to be 75.4 nm. The TEM image in Figure 4.3A shows that CNDs are closely related and this indicates that they have a graphitic nature.

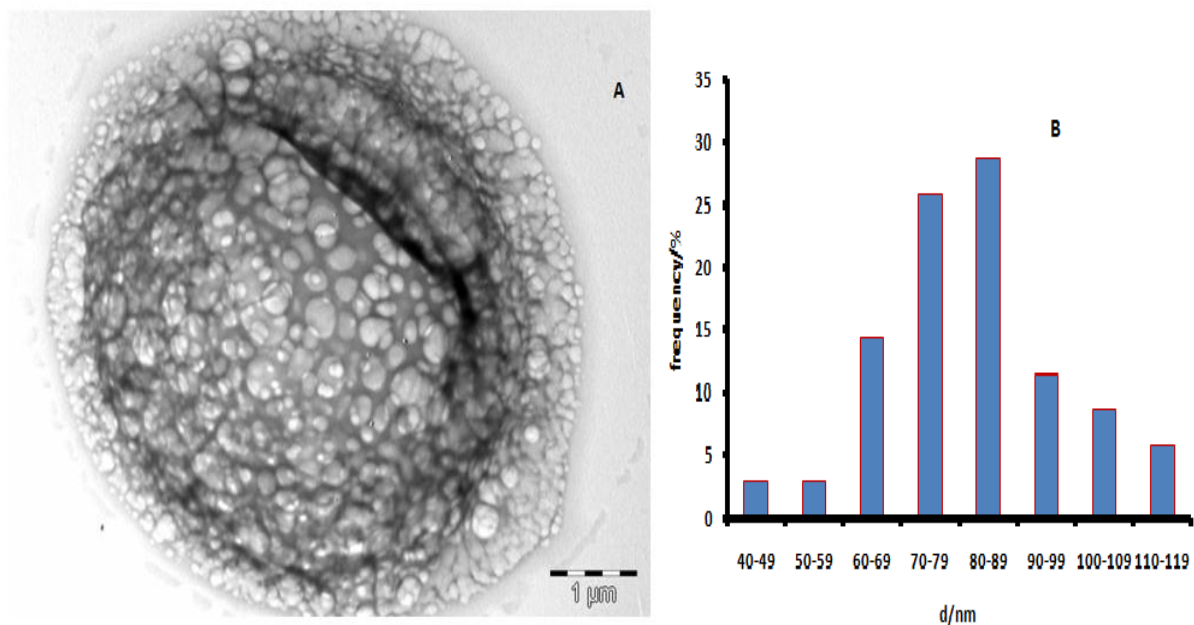


Fig 4.3: (A) TEM image of CNDs and (B) diameter distribution of the CNDs

## 4.4 Electrochemical Characterization

### 4.4.1 Cyclic Voltammetry.

Electrochemical behavior of modified electrodes in redox probe by cyclic voltammetry in 1 mM  $[\text{Fe}(\text{CN})_6]^{3-/4-}$  solution containing 0.1 M KCl at 0.1 V/s are shown in Figure 4.4. The peak potential separation ( $\Delta E_p$ ) for a reversible system such as  $\text{Fe}(\text{CN})_6^{3-/4-}$  is a good measure of the electron transfer ability of the electrode with lower values depicting a good electron transfer ability, which follows the following order: CoTAPhPcNPs n-CNDs /-GCE = (0.0718 V) > CoTAPhPcNPs/CNDs-GCE (0.0738 V) > CoTAPhPcNPs -GCE (0.0762 V) > Bare GCE (0.0784 V) > n-CNDs-GCE (0.1245 V) > CNDs-GCE (0.2515 V), Table 1. It can be noted that n-CNDs and CNDs have the worst electron transfer ability because of the poor electroactive properties.

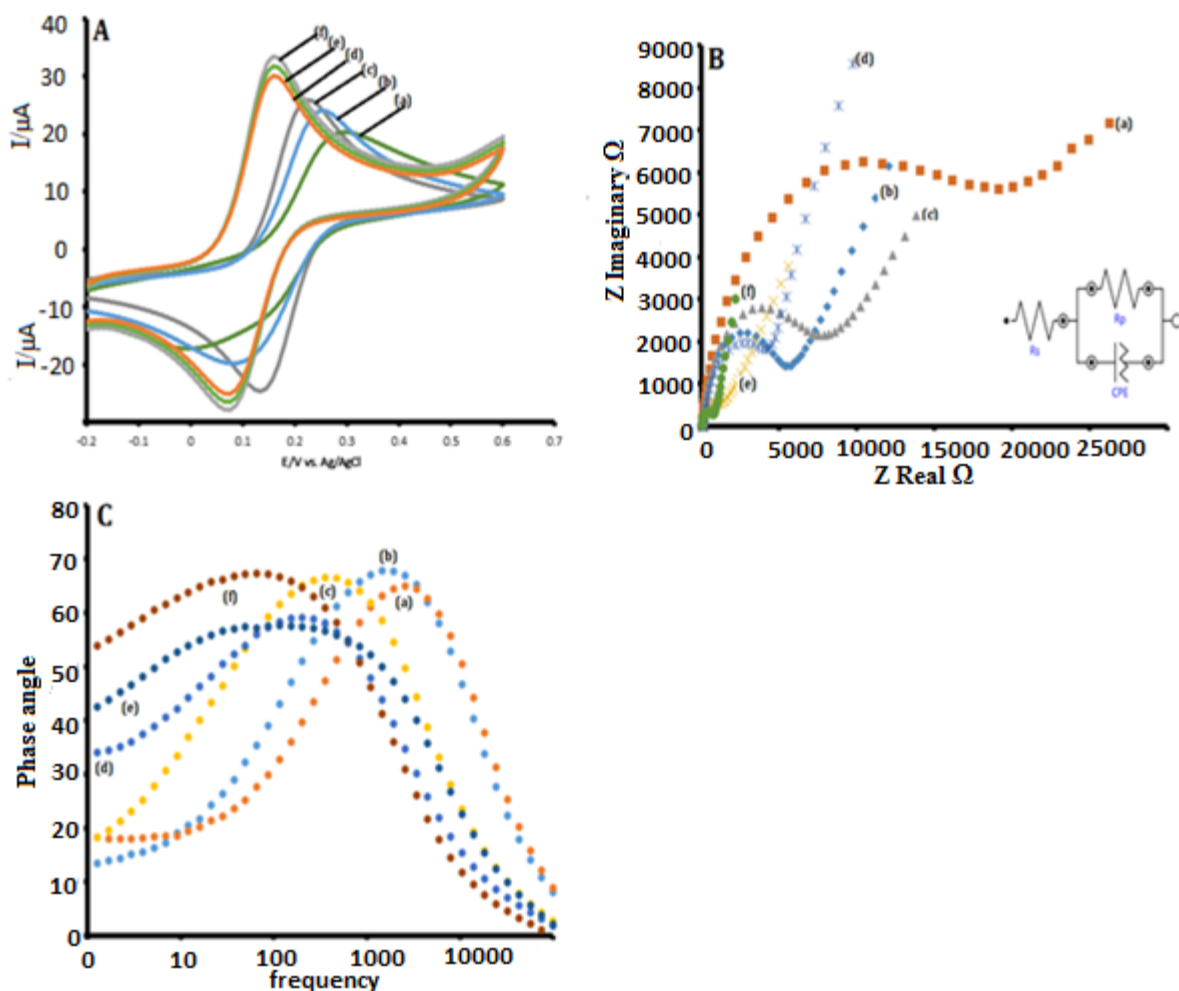


Fig 4.4: (A) CVs in 1mM Ferri/Ferro in 0.1M KCl, (a) CNDs-GCE, (b) n- CNDs-GCE, (c) Bare-GCE, (d) CoTAPhPcNPs-GCE (e) CoTAPhPcNPs/CNDs-GCE (f) CoTAPhPcNPs/n-CNDs-GCE (B) Nyquist plots in 1mM Ferri/Ferro in 0.1M KCl, (C) Bode plots in 1mM Ferri/Ferro in 0.1M KCl

Modification of the bare electrode by all the modifiers except for n-CNDs and CNDs results in the improvement of the electrode conductivity (table 4. 1). Incorporation of cobalt tetra amino phenoxy phthalocyanine nanoparticles results in improved electron transfer ability because they facilitate the movement of electron due to presence of catalytic metal centre and the amino phenoxy group on the peripheral end of phthalocyanine. The n-CNDs with peak to peak

separation of 0.1245 V, they behaved poorly compared to CoTAPhPcNPs/n-CNDs with peak to peak separation of 0.0718V. There was increase in current from the CNDs-GCE to CoTAPhPcNPs/n-CNDs-GCE in Figure 4.3A. The increase in current shows increase in sensitivity. The surface roughness factors for the modified electrodes were determined using  $[\text{Fe}(\text{CN})_6]^{3-/4-}$  redox system and applying Randles–Sevcik equation for reversible systems :

$$I_p = 2.69 \times 10^5 n^{3/2} A C D^{1/2} V^{1/2} \quad (4.1)$$

where  $I_p$ ,  $n$ ,  $A$ ,  $C$ ,  $D$  and  $v$  are the peak current, the number of electrons involved, the surface area, the concentration of  $[\text{Fe}(\text{CN})_6]^{3-/4-}$ , the diffusion coefficient of  $[\text{Fe}(\text{CN})_6]^{3-/4-}$ , and the scan rate, respectively. From the  $D$  value for  $\text{K}_3[\text{Fe}(\text{CN})_6] = 7.6 \times 10^{-6} \text{ cm}^2 \text{ s}^{-1}$  and  $n = 1$ . The surface roughness factors of the electrodes were determined using the formula: ratio of  $I_{pa}$  experimental/ $I_{pa}$  theoretical and it can be estimated based on Randles–Sevcik equation [37]. The values are given in table 4.1 were determined for all the probes and the results showed that there is increased roughness for CoTAPhPcNPs/n-CNDs-GCE electrode compared to CNDs-GCE. The real electrode areas were calculated using the formula: roughness factor  $\times$  theoretical surface area ( $0.071 \text{ cm}^2$ ). The real electrode area for CoTAPhPcNPs/n-CNDs-GCE is two times larger than the bare electrode area  $0.071 \text{ cm}^2$ . Therefore, the CoTAPhPcNPs/n-CNDs-GCE is expected to perform better than all electrodes based on effective electrode area. The table below gives a summary of the parameters in cyclic voltammetry.

#### 4.4.2 Nyquist plots

Figure 4.4B shows Nyquist plots obtained for the modified electrodes in 1 mM  $[\text{Fe}(\text{CN})_6]^{3-/4-}$  and in 0.1 M of KCl. Inset is the Randles circuit model used in fitting the data. Electrochemical Impedance Spectroscopy is a complex process that gives insightful information about reaction at

the electrode-electrolyte interface and it is a strong evidence for studying the interface feature of the modified electrodes [38]. The results obtained include semi-circular portions corresponding to the electron-transfer-limited process and a linear part resulting from the diffusion controlled process [39]. The diameter of the semicircle corresponds to the charge transfer resistance ( $R_{ct}$ ) of the redox probe at the electrode interface.

Table 4.1: Electrochemical parameters for the modified electrodes.

Electrode	$\Delta E_p$ for $FeCN_6^{3-/4-}$	Surface roughness factor	Effective electrode area	Surface coverage ( $cm^{-2}$ )	$R_{ct}$ (k $\Omega$ )	$K_{app}$
Bare-GCE	0.078	-	-	-	8.3	-
CNDs-GCE	0.2515	1.177	0.0836	-	22.603	$1.4 \times 10^{-7}$
n-CNDs-GCE	0.124	1.393	0.0989	-	9.14	$2.94 \times 10^{-7}$
CoTAPhPcNPs GCE	0.0762	1.839	0.1305	$3.2 \times 10^{-8}$	5.61	$3.63 \times 10^{-7}$
CoTAPhPcNPs/CNDs-GCE	0.0738	1.862	0.1322	$3.4 \times 10^{-8}$	1.51	$1.333 \times 10^{-6}$
CoTAPhPcNPs/n-CNDs-GCE	0.0718	1.934	0.1373	$3.8 \times 10^{-8}$	1.36	$1.425 \times 10^{-6}$

A smaller  $R_{ct}$  value implies that the probe has a higher interfacial electron transfer rate. The circuit model used in the fitting of the impedance data is represented in Figure 4.4B. In this circuit model,  $R_s$  is the solution resistance,  $R_{ct}$  is the charge transfer resistance. From the  $R_{ct}$  values in table 4.1, the order of increasing electron transport is as follows: CNDs-GCE (22.6 k $\Omega$ ) < n-CNDs-GCE (9.14 k $\Omega$ ) < BGCE (8.3 k $\Omega$ ) < CoTAPhPcNPs-GCE (5.6 k $\Omega$ ) < CoTAPhPcNPs/CNDs-GCE (1.51 k $\Omega$ ) < CoTAPhPcNPs/n-CNDs-GCE (1.36 k $\Omega$ ). The electron transport is faster for CoTAPhPcNPs/n-CNDs-GCE electrode compared to others. The CNDs

GCE exhibited a large semicircle with a  $R_{ct}$  value of 22.6 k $\Omega$ , revealing the slow electron transfer. Therefore, CoTAPhPcNPs/n-CNDs-GCE electrode showed a rapid electron transfer and it can be ascribed to be the excellent electron conductor. The  $n$  values are less than ideal 1.0 expected from an ideal capacitive behavior, therefore suggesting pseudo-capacitive properties for these electrodes. The apparent rate constant ( $K_{app}$ ) for all electrodes was obtained by using the equation:

$$K_{app} = RT/n^2F^2R_{ct}AC \quad (4.2)$$

Where  $C$  is the concentration of the Ferri/Ferro(1mm),  $R_{ct}$  (charge transfer resistance) from fitted data,  $A$  is the real electrode area,  $n$  = electron involved in the redox process, with  $R$ ,  $T$  and  $F$  have their usual meaning [40]. The  $K_{app}$  value is attributed monolayer coverage on the surface of the electrode thus blocking the solution ions from reaching the surface. The solution blocking effect was worse on the CNDs GCE ( $1.4 \times 10^{-7}$ ) and n-CNDs GCE ( $2.94 \times 10^{-7}$ ). When MPc complexes (CoTAPhPcNPs) are immobilized onto CNDs and n-CNDs surfaces, forming CoTAPhPcNPs/CNDs and CoTAPhPcNPs/n-CNDs monolayers, the  $K_{app}$  value increased to  $1.333 \times 10^{-6}$  and  $1.425 \times 10^{-6}$  respectively. The increase of the  $K_{app}$  value could be attributed to the conducting and electrocatalytic properties of cobalt tetra amino phenoxy phthalocyanine nanoparticles. The combination of the CNDs materials and metalphthalocyanine nanoparticles clearly shows an increase in the apparent electron transfer constant.

#### 4.4.3 Bode Plots

Figure 4.4C shows bode (phase angle versus log  $f$ ) plots obtained for (a) CNDs-GCE (b)n-CNDs-GCE (c) BGCE (d) CoTAPhPcNPs-GCE (e) CoTAPhPcNPs/CNDs-GCE (f) CoTAPhPcNPs/n-CNDs-GCE. Nyquist plots cannot reveal frequency related information, however this information is then obtained from the bode plots. The nature of bode plots

confirmed structural differences of the modified electrodes. After modification of the glassy carbon electrode with CNDs, n-CNDs, CoTAPhPcNPs, CoTAPhPcNPs/CNDs and CoTAPhPcNPs/n-CNDs, the peaks shifted to lower frequencies indicating that electrocatalysis is occurring at the surface of the electrode. Phase angles were decreasing and they were less than the ideal  $90^{\circ}$  for an ideal capacitor.

#### 4.5 Surface Coverage

The surface coverage of the modified electrodes was determined from Figure 4.5 using the equation 4.3

$$I_{pa} = \frac{n^2 F^2 v A_e \Gamma}{4RT} \quad (4.3)$$

where  $\Gamma$  is the surface coverage,  $I_{pa}$  is the anodic peak current,  $R$  is the molar gas constant,  $T$  is the temperature,  $n$  is the number of transferred electrons,  $F$  is the Faraday constant,  $A_e$  is the electrode surface area and  $V$  is the scan rate. The surface coverages of all electrodes in media follow the order CoTAPhPcNPs/n-CNDs-GCE > CoTAPhPcNPs/CNDs-GCE > CoTAPhPcNPs-GCE. There is poor electron transfer ability for CoTAPhPcNPs-GCE since it has lower surface coverage to the rest of electrodes. Lower surface coverage suggest different orientation compared to the rest of electrode modifiers [9].The summary is given in table 4.1.

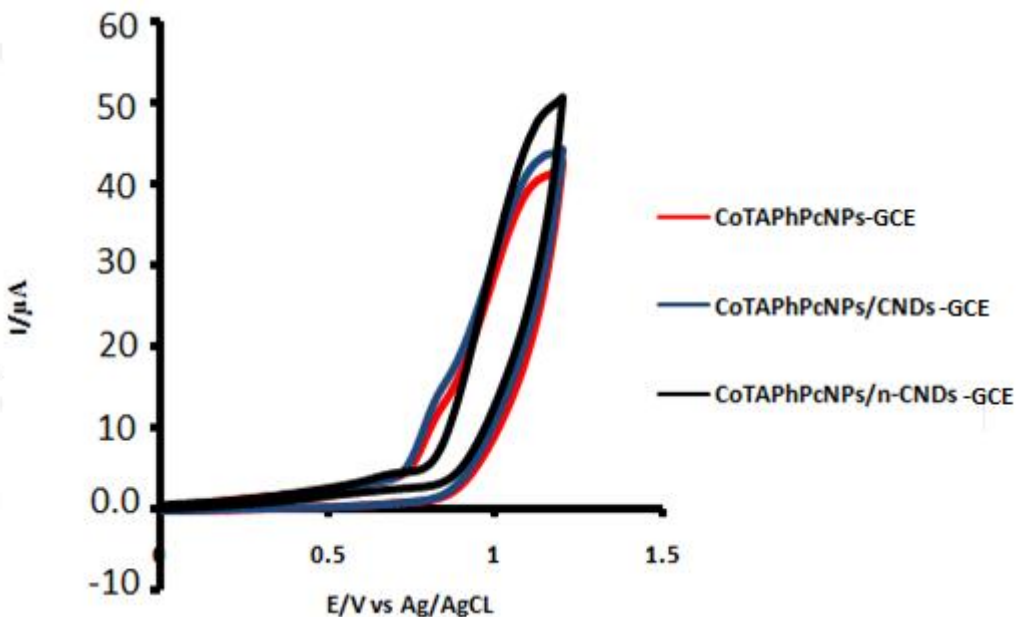


Fig 4.5: Cyclic voltammograms of the modified electrodes in pH 6 phosphate buffer solution. Scan rate 100mV/s

## 4.6 Electrocatalytic detection of the Drugs

### 4.6.1 pH optimization

Voltammograms of aspirin, ibuprofen and indomethacin were recorded at various pH between 3 and 8 at scan rate of 0.1V. Oxidation peaks were observed in different pH. The influence of pH on the oxidation of the three compounds was studied in phosphate buffer. Figure 4.6 shows the effect of pH on the peak potential and peak current values. Variation of peak current with pH resulted in a parabolic curve. Maximum peak current for oxidation of ASA, IBU and INDO was observed at pH4, pH5 and pH6 respectively. This may be due to the faster electron transfer at acidic pH and this indicates that the rate of reaction is controlled only by one electron transfer.

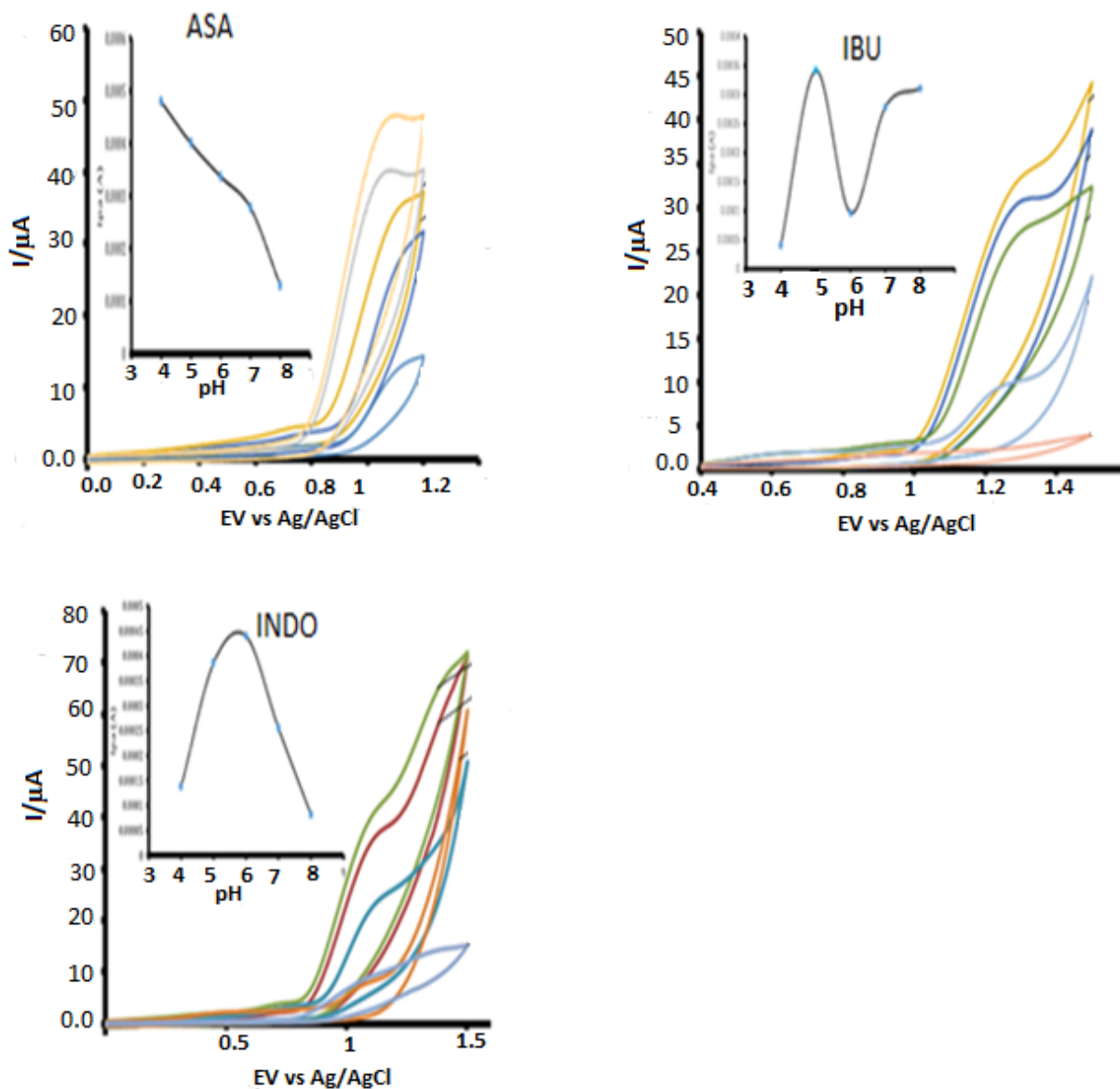


Fig 4.6: Optimization of Ph for each analyte in PBS. Scan rate 100mV/s

As the pH for ASA and INDO increased beyond 7.0 the peak current decreased and above pH 7.0, there is a distortion in the peak shape. Furthermore, as the pH was increased above 7.0 the oxidation of aspirin and indomethacin became kinetically less favorable. From the study, it is concluded that pH 4 for ASA, pH 5 for IBU and Ph 6 for INDO were the optimum pH for electrochemical process.

#### 4.6.2 Electrocatalytic Detection of the ASA, IBU and INDO

The cyclic behavior of ASA, IBU and INDO in Figure 4.7 was studied at CoTAPhPcNPs GCE, CoTAPhPcNPs/CNDs-GCE and CoTAPhPcNPs/n-CNDs-GCE modified electrodes. Anodic peaks were observed in the potential range from 0 to 1.5V. The anodic peak observed in Figure 4.7 at 0.815V is accounted for oxidation of aspirin. The anodic peak potential observed at 1.318V is accounted for the oxidation of ibuprofen and the anodic peak potential observed at 1.003V is accounted for the oxidation of indomethacin. In the applied potential range, there was a reduction in potential from CoTAPhPcNPs GCE to CoTAPhPcNPs/n-CNDs-GCE (table 4. 2). The CoTAPhPcNPs/n-CNDs-GCE shows superior currents in all the compounds despite a slightly higher oxidation overpotential compared to CoTAPhPcNPs GCE and CoTAPhPcNPs/CNDs-GCE which have low oxidation currents. The reasons for the excellent electro-catalytic performance towards oxidation ASA, IBU and INDO at CoTAPhPcNPs/n-CNDs-GCE may be deduced as the numerous catalytic active sites and efficient electrical network for oxidation of ASA, IBU and INDO are afforded by the high loading and well distributed CoTAPhPcNPs on n-CNDs surface. The pyridinic N at n-CNDs can give a pair of electrons for conjugation with the pi- conjugated rings, introducing electrons donor to n-CNDs and improving the electrochemical behavior of n-CNDs. Furthermore, the pyrrolic N has charge mobility in n-CNDs because of the considerable electron –donor properties and strengthens the carbon electro-catalytic activity in electron transfer reactions. Therefore, the electro-catalytic activity of CoTAPhPcNPs/n-CNDs-GCE is trusted to be better than pure CoTAPhPcNPs GCE. Without a doubt, the synergistic effect CoTAPhPcNPs and n-CNDs makes the excellent electron-catalytic activity toward the oxidation of ASA, IBU and INDO.

Table 4.2: Electrochemical parameters of the modified electrodes for each analyte

Molecule	Electrode	Ipa( $\mu$ A)	Epa(mV)	Background corrected( $\mu$ A)	Rct (k $\Omega$ )	Kapp
ASA	CoTAPhPcNPs GCE	283.6	0.847	293	3.388	$6.01 \times 10^{-7}$
	CoTAPhPcNPs/CNDs-GCE	319	0.832	306.8	1.645	$1.22 \times 10^{-6}$
	CoTAPhPcNPs/n-CNDs-GCE	437	0.8156	411	1.328	$1.459 \times 10^{-6}$
IBU	CoTAPhPcNPs GCE	135	1.331	67	3.461	$5.89 \times 10^{-7}$
	CoTAPhPcNPs/CNDs-GCE	156	1.322	83.9	1.528	$1.317 \times 10^{-6}$
	CoTAPhPcNPs/n-CNDs-GCE	233	1.318	229.4	1.273	$1.52 \times 10^{-6}$
INDO	CoTAPhPcNPs GCE	282	1.045	255.7	3.764	$5.41 \times 10^{-7}$
	CoTAPhPcNPs/CNDs-GCE	322	1.035	305.6	1.742	$1.15 \times 10^{-6}$
	CoTAPhPcNPs/n-CNDs-GCE	394	1.003	367.5	1.355	$1.43 \times 10^{-6}$

### 4.6.3 Electrochemical impedance spectroscopy studies of aspirin, ibuprofen and indomethacin

EIS was employed for the characterization of CoTAPhPcNPs GCE, CoTAPhPcNPs/CNDs-GCE and CoTAPhPcNPs/n-CNDs-GCE for each analyte in phosphate buffer in attempt to clarify structural differences among electrochemical performance. The circuit models used in the fitting of the impedance data is represented in Figure 4.7 for each analyte. Figure 4.7 shows Nyquist plots obtained for (a) CoTAPhPcNPs-GCE (b) CoTAPhPcNPs/CNDs-GCE (c) CoTAPhPcNPs/n-CNDs-GCE in (A) ASA, (B) IBU and (C) INDO. In all analytes, a large semicircle was observed at CoTAPhPcNPs GCE. The charge transfer resistance (Rct) decreased from CoTAPhPcNPs GCE to CoTAPhPcNPs/n-CNDs in each analyte. The order of decreasing the Rct value is as follows: CoTAPhPcNPs GCE > CoTAPhPcNPs/CNDs-GCE >

CoTAPhPcNPs/n-CNDs-GCE. The  $R_{ct}$  value was the smallest at CoTAPhPcNPs/n-CNDs-GCE compared to all electrodes (Table 4.2). This was due to facilitation of the electron transfer by electrode modifiers. The plots of CoTAPhPcNPs/n-CNDs-GCE in all analytes have the lowest charge transfer resistance that is smallest diameters, this decrease in  $R_{ct}$  values at CoTAPhPcNPs/n-CNDs-GCE is attributed to (i) CoTAPhPcNPs being a good conductor of electrons and (ii) the combination of electrocatalytically active materials with low active materials (n-CNDs and CoTAPhPcNPs) have synergistic effects in terms of enhancing electron transfer to and from the electrode surface. These charge transfer resistance values show that ASA, IBU and INDO are oxidized at lower potentials which is in agreement with cyclic voltammetry. The apparent electron transfer rate constant was obtained from the conventional equation. This method investigates the outer sphere kinetic properties of the immobilized thin films and their interaction with the redox probe in solution. The  $K_{app}$  for ASA, IBU and INDO were obtained by using the equation 4.2. The apparent electron transfer rate constants at CoTAPhPcNPs GCE and CoTAPhPcNPs/CNDs-GCE were slightly low in ASA, IBU and INDO ranging from  $5.41 \times 10^{-7}$  to  $6.01 \times 10^{-7} \text{ cm s}^{-1}$  and  $1.15 \times 10^{-6}$  to  $1.317 \times 10^{-6} \text{ cm s}^{-1}$  respectively, compared to CoTAPhPcNPs/n-CNDs-GCE ranging from  $1.43 \times 10^{-6}$  to  $1.522 \times 10^{-6} \text{ cm s}^{-1}$ . The slight decrease in  $K_{app}$  value is due to monolayer coverage on the electrode thus blocking the solution ions from reaching the electrode surface. The solution blocking effect was much less at CoTAPhPcNPs GCE. When two materials are combined together (n-CNDs and CoTAPhPcNPs), there was an increase in  $K_{app}$  value in all analytes.

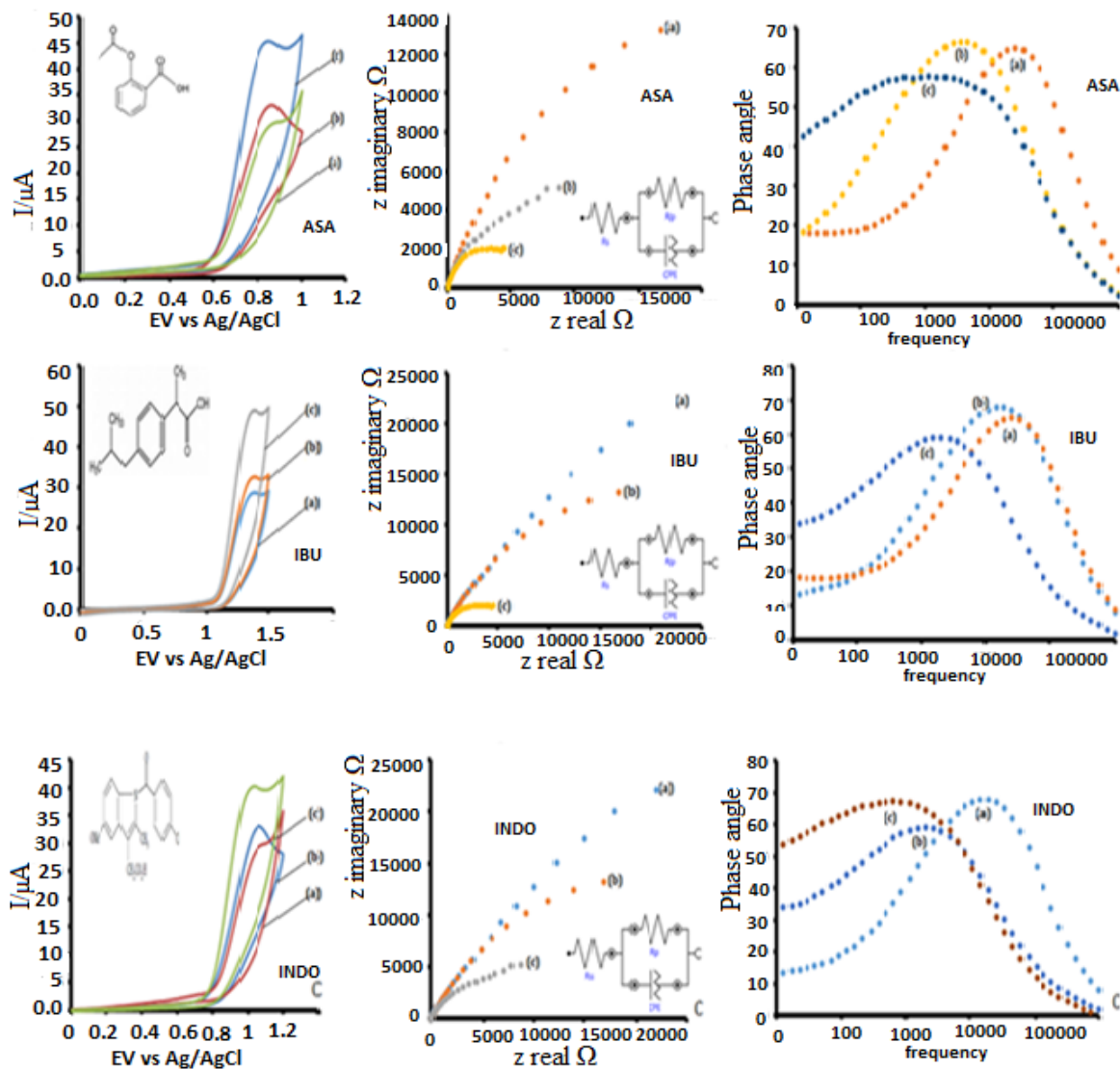


Fig 4.7: CVs, Nyquist plots and Bode plots for ASA, IBU and INDO, (a) CoTAPhPcNPs-GCE, (b) CoTAPhPcNPs/CNDs-GCE, (c) CoTAPhPcNPs/n-CNDs-GCE

#### 4.6.4 Bode plots

Bode plots were used to obtain frequency related information, which cannot be obtained from their Nyquist plots. Figure 4.7 shows bode plots obtained for (a) CoTAPhPcNPs-GCE (b) CoTAPhPcNPs/CNDs-GCE (c) CoTAPhPcNPs/n-CNDs-GCE in ASA, IBU and INDO. The nature of the Bode plots confirmed the structural differences of the GCE modified electrodes in

ASA, IBU and INDO. All the peaks have lower frequencies for the relaxation processes of the modifier GCE interfaces. The relaxation process of the CoTAPhPcNPs/n-CNDs-GCE in ASA, IBU and INDO was at a phase angle of 55, 59 and 64 respectively. Changes in phase angle and frequencies confirmed that the oxidation of ASA, IBU and INDO was taking place at modified platform. Both the Nyquist and the Bode plots confirmed the good electron transfer kinetics at the CoTAPhPcNPs/n-CNDs-GCE for ASA, IBU and INDO. Such a trend was also observed from the cyclic voltammetry of ASA, IBU and INDO on the same electrode where CoTAPhPcNPs/n-CNDs-GCE showed reduced potentials and improved currents. At the frequency region of the impedance under study the charge transfer  $R_{ct}$ , decreased for the electrode modifiers due to facilitation of the electron transfer which is an indication that films form high electron conduction pathways between the electrode and electrolyte /analyte. The phase angles values for all electrode surfaces in all analytes studied in this work are less than the ideal  $90^\circ$  for a true capacitor.

#### **4.6.5 Simultaneous cyclic voltammetry studies**

Composite solution were prepared as follows 1mM each of ASA and IBU, 1mM each of ASA and INDO, 1mM each of IBU and INDO and 1mM each of ASA, IBU and INDO. The results are presented in Figure 4.8. In all composites containing ASA, only peaks for either IBU or/and INDO were observed. In conclusion, the developed sensor could not peak ASA in the presence of other analyte.

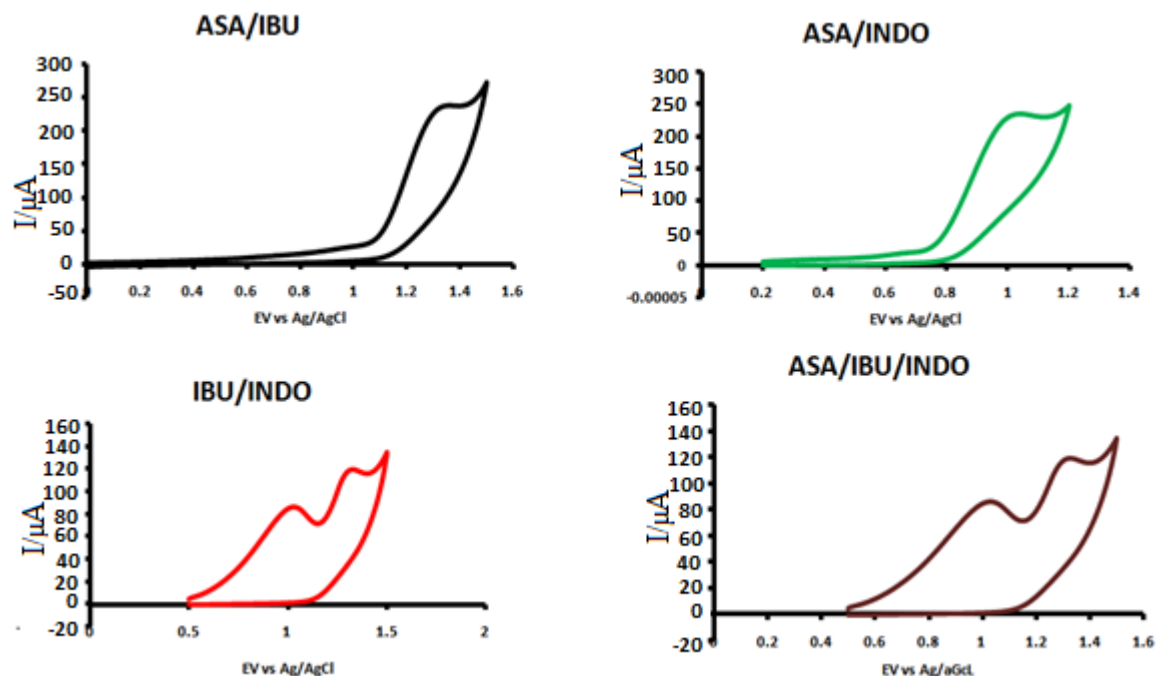


Fig 4.8: Simultaneous Cyclic voltammograms responses in 1mM ASA/IBU, 1mM ASA/INDO, 1mMIBU/INDO, 1mM ASA/IBU/INDO in PBS.

#### 4.6.6 Kinetic Studies

The influence of scan rate plays an important role in voltammetric oxidation reactions. Useful information involving electrochemical mechanism could be acquired from the relationship between peak current and scan rate[2]. The influence of changing scan rate over the range 50-400mV/s was studied to detect diffusion and adsorption properties[41] of 1mM ASA, 1mM IBU and 1mM INDO using CoTAPhPcNPs/n-CNDs-GCE. It can be seen that anodic peak currents were increasing with increase in scan rate in Figure 4.9 [42]. Furthermore, the anodic peak current in all analytes showed linear relationship with the scan rate from 50 to 400mV/s suggesting that at sufficient overpotential, the process is diffusion controlled rather than surface

controlled. The regression equations for all analytes at CoTAPhPcNPs/n-CNDs-GCE are as follows:

$$I_p = 3 \times 10^{-5}v + 8 \times 10^{-5}; R^2 = 0.9914(\text{ASA})$$

$$I_p = 1 \times 10^{-5}v + 0.0002; R^2 = 0.9891(\text{IBU})$$

$$I_p = 3 \times 10^{-5}v + 0.0001; R^2 = 0.9949(\text{INDO})$$

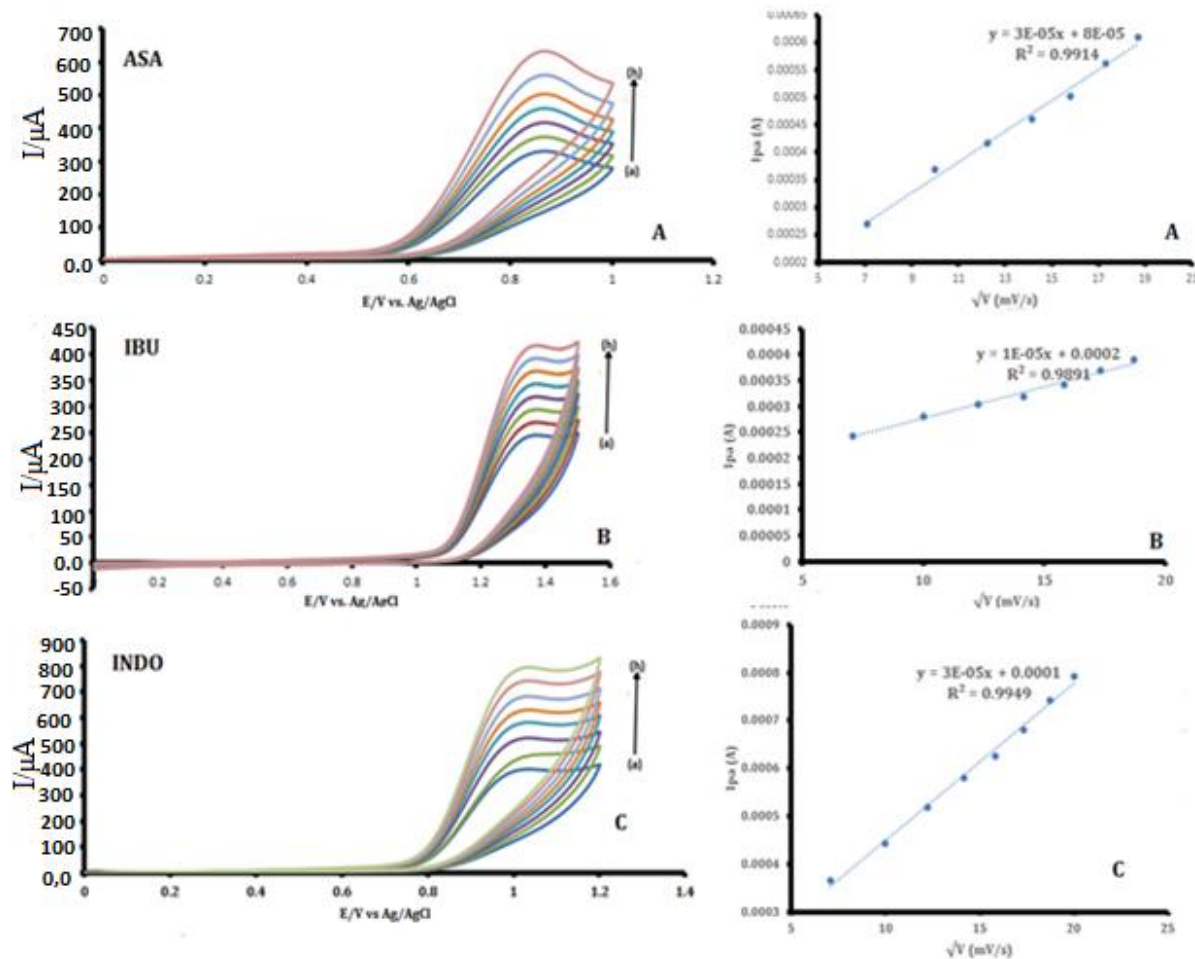


Fig 4.9: Effect of scan rate on peak potentials and currents a) 50mV/s b) 100 mV/s, c) 150 mV/s, d) 200 mV/s, e) 250 mV/s, f) 300 mV/s, g) 350 mV/s, h) 400 mV/s on CoTAPhPcNPs/n-CNDs-GCE for ASA, IBU and INDO oxidation.  $[ ] = 1\text{mM}$ . *Inset*: plot of  $I_{pa}$  vs  $\sqrt{v}$ .

#### 4.6.7 Tafel slopes

For an electrochemically irreversible electro oxidation process the value of Tafel slope can be obtained from the variation of  $E_{pa}$  with  $V$  in voltammetric data through equation[43]

$$E_{pa} = b \log V/2 + K \quad (4.4)$$

$$\text{The value of } b \text{ is } 2.303RT/(1-\alpha)n\alpha F \quad (4.5)$$

where  $E_{pa}$  is the oxidation peak potential,  $K$  = constant  $\alpha$  = electron transfer coefficient,  $n$  = number of electrons transferred in the rate determining step,  $v$  = scan rate,  $R$  = molar gas constant (8.314) and  $T$ = temperature(298K). The value of Tafel slope ( $b$ ) gives an idea about the number of electrons transferred in the rate determining step. Figure 4.10 shows a linear plot of peak potential,  $E_p$  versus  $\log v$ . An increase in scan rate from 50 to 400 mV/s resulted in the oxidation peak shifting towards positive potentials indicating the chemical irreversibility of the electrocatalytic oxidation processes of ASA, IBU and INDO. Plots of  $E_p$  versus  $\log v$  gave a linear relationship as represented by the equation. Tafel slopes obtained for ASA, IBU and INDO are 180, 233 and 213 mV decade<sup>-1</sup> respectively. Tafel slopes of this magnitude have no kinetic meaning but could indicate a passivated phenomenon occurring on the electrode surface. Tafel slopes much greater than the normal 60-120 mV decade<sup>-1</sup> for a one electron rate determining step have been observed in all analytes and have been either to chemical reaction coupled to electrochemical steps or to substrate catalyst interactions in a reaction intermediate. Similar Tafel slopes have been observed in systems involving species with very high surface to volume ratio, like MPc.

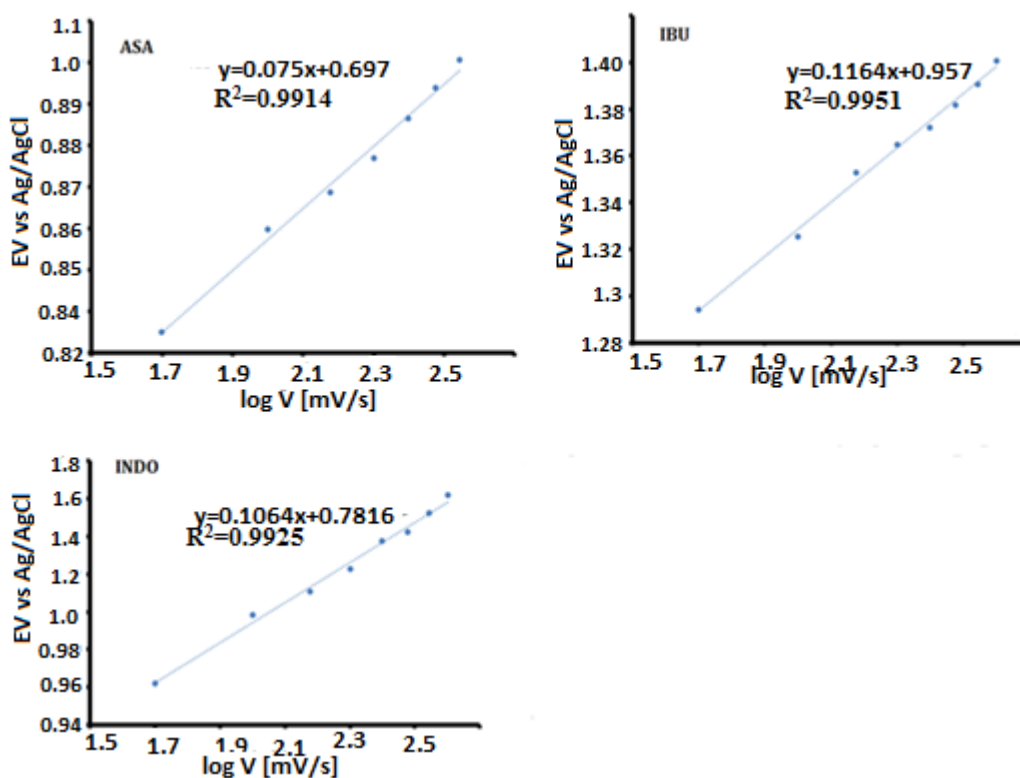


Fig 4.10: Plot of potential versus log scan rate in 1mM (A) ASA, (B) IBU and (C) INDO

#### 4.6.8 Order of reaction

The plots in fig 4.11 show a linear relationship in all analytes and from these plots, the order of reaction can also be deduced or estimated. The correlation values for ASA, IBU and INDO were 0.9947, 0.9912 and 0.9907 respectively giving evidence that there was linear relationship between log concentration and log of current. The electro catalysis of ASA was found to be first order from the plot log  $I_{pa}$  versus log [ASA], implying that one analyte molecule interacts with one molecule of CoTAPhPcNPs/n-CNDs. The electro catalysis of both IBU and INDO were also found to be first order.

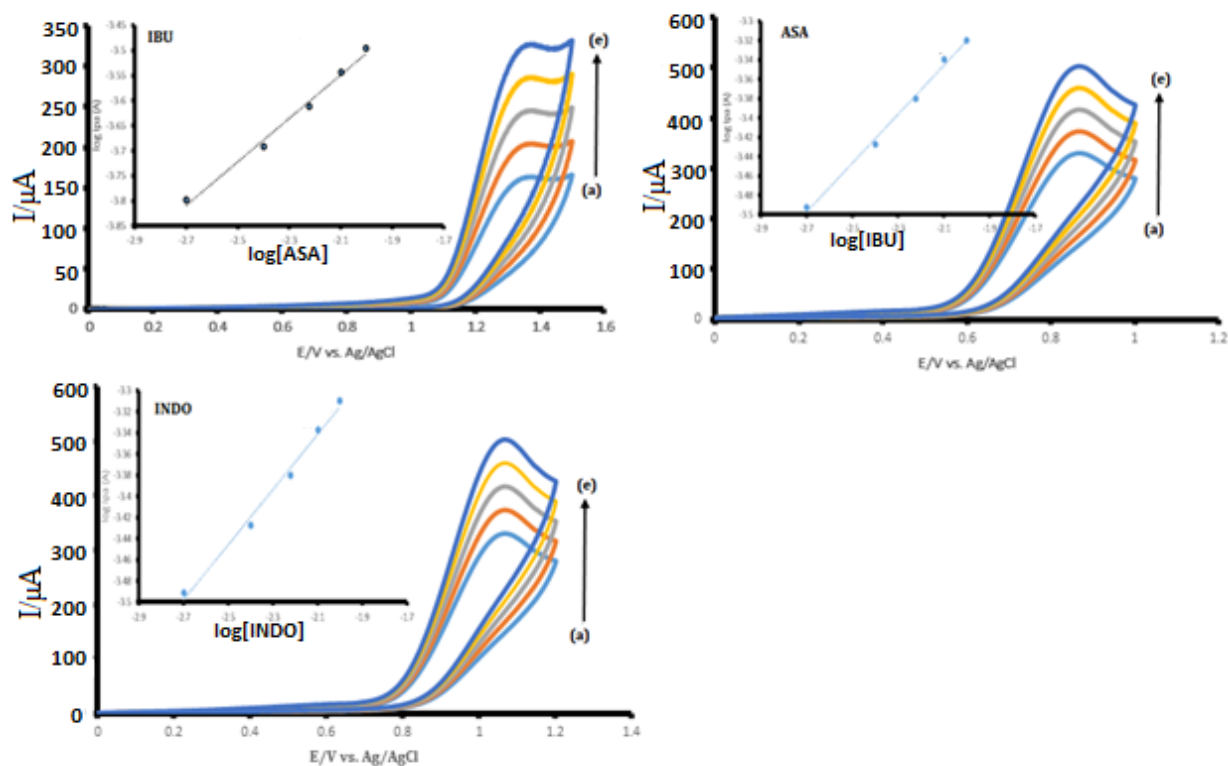


Fig 4.11: Cyclic voltammograms for (a) 5 mM , (b) 10mM, (c) 15mM (d) 20mM and (e) 25mM of ASA (pH 4), IBU (pH 5) and INDO (pH 6) concentrations in PBS. *Inset* plot of  $\log I_{pa}$  vs  $\log [ASA, IBU, INDO]$

#### 4.6.9 Determination of Gibbs' energy

Linear sweep voltammetry (LSV) was conducted in order to show adsorption behavior of CoTAPhPcNPs/n-CNDs-GCE. Fig 4.12 shows LSV plots obtained and the Langmuir adsorption theory was applied. A plot of the ratio of ASA, IBU and INDO concentrations to catalytic current against concentration of each analyte gave a linear plot which is indicative of adsorption. Equation 3.1 was used to determine  $\beta$  that is the adsorption equilibrium constant. From the slope and the intercept of (Figure 4.12), the adsorption equilibrium constant ( $\beta$ ) for ASA, IBU and INDO were established to be  $1.05 \times 10^5 M^{-1}$ ,  $1.2 \times 10^5 M^{-1}$  and  $5.56 \times 10^5 M^{-1}$  respectively. The

values of the adsorption equilibrium constant correlate with those in literature [9]. High Tafel slopes obtained in this study shows adsorption of each analyte to the surface of the electrode. Using equation 3.2 which relates Gibbs free energy change due to adsorption ( $\Delta G^\circ$ ) equilibrium constant  $\beta$ ,  $\Delta G^\circ$  for ASA, IBU and INDO were found to be  $-28.63\text{KJ mol}^{-1}$ ,  $-28.96\text{KJ mol}^{-1}$  and  $-27.07\text{KJ mol}^{-1}$  respectively. The values obtained for each analyte are very high and this indicates the spontaneity of the reactions.

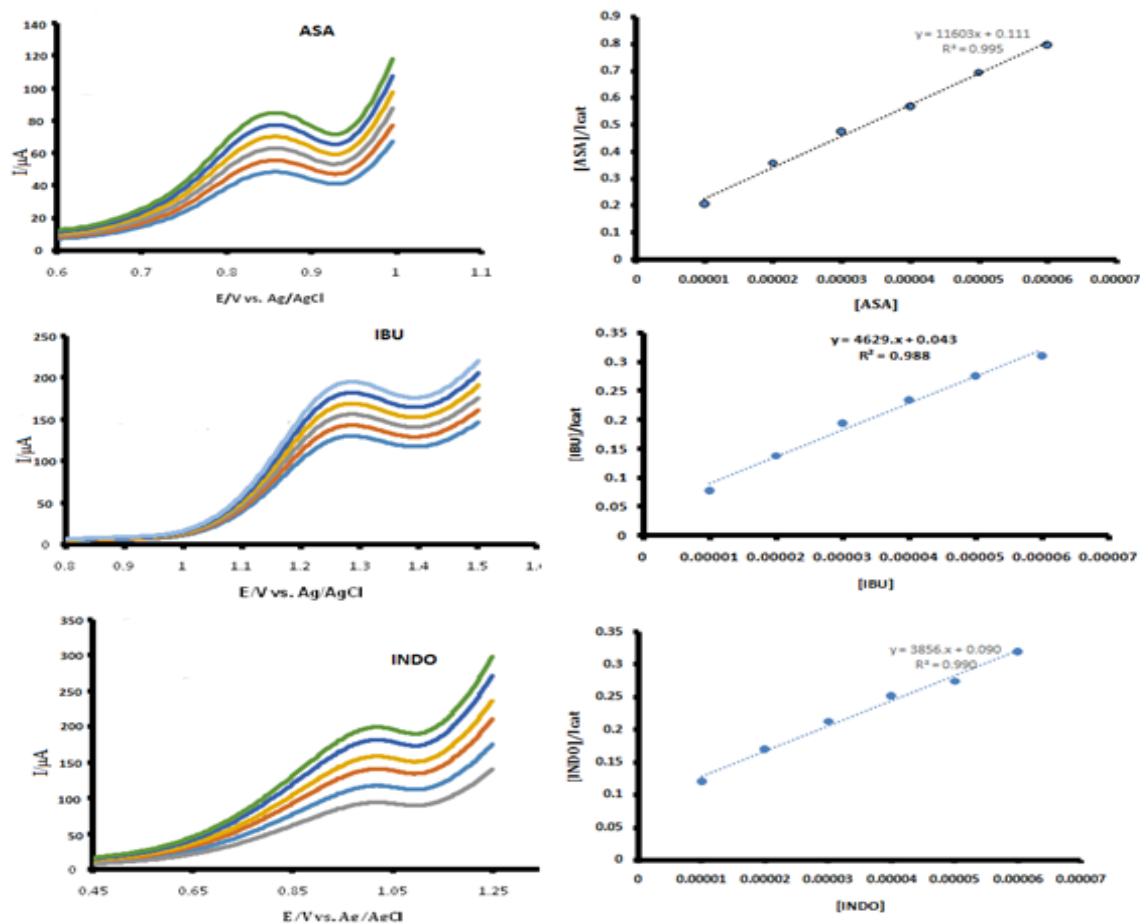


Fig 4.12: Linear sweep voltammograms and Langmuir adsorption isotherm plot for CoTAPhCnPs/n-CNDs-GCE (10  $\mu\text{M}$ , 20  $\mu\text{M}$ , 30  $\mu\text{M}$ , 40  $\mu\text{M}$ , 50  $\mu\text{M}$ , 60  $\mu\text{M}$ ) of ASA, IBU and INDO concentrations in PBS.

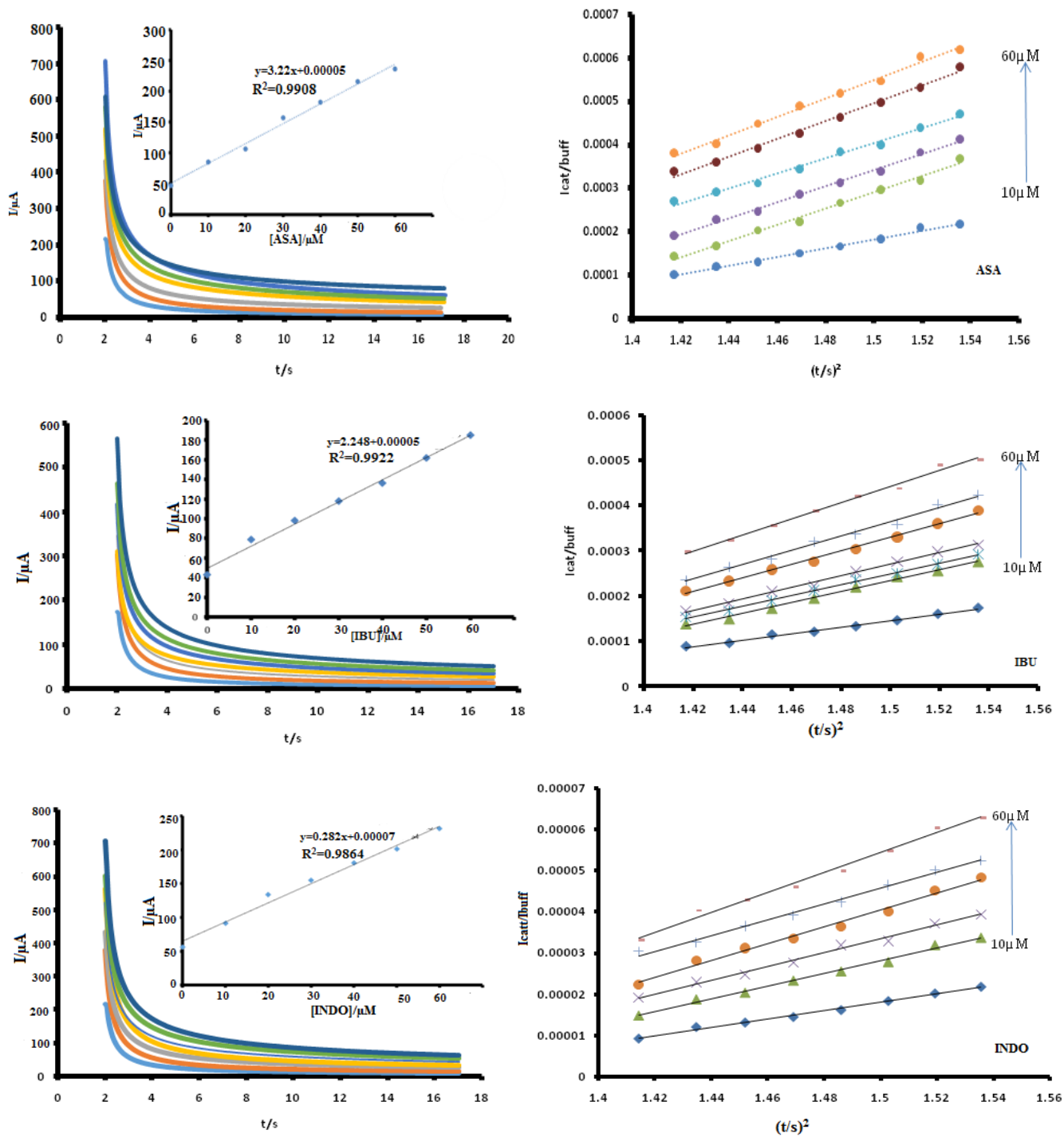


Fig 4.13: Chronoamperograms (Insert-dependence concentration on current) and plots of  $I_{cat}/I_{buff}$  versus  $t^{1/2}$  (10-60 $\mu$ M) in PBS determined using chronoamperometry for CoTAPhPcNPs/n-CNDs-GCE.

#### 4.6.10 Determination of catalytic rate constant

Chronoamperometric curves in Figure 4.13 were utilized to determine [44] ASA, IBU and INDO at CoTAPhPcNPs/n-CNDs-GCE. The steady-state amperometric response of the modified electrode was investigated by successive addition of amount of ASA, IBU and INDO in phosphate buffer pH4, pH5 and pH6 respectively under the optimal conditions. The n-CoTAPhPcNPs/n-CNDs-GCE modified electrode exhibited a fast response to the change in concentration of each analyte (Figure 4.13). After increasing the concentration of each analyte response current immediately enhanced. When the concentration of ASA, IBU and INDO increases from 10 to 60  $\mu\text{M}$ , the current response corresponding to the concentration has a linear relationship (Figure 4.13). The rate constants for the detection of ASA, IBU and INDO were calculated using the equation:

$$\frac{I_{cat}}{I_{buf}} = \pi^{\frac{1}{2}}(kC_0t)^{1/2} \quad (4.6)$$

Where  $I_{cat}$  and  $I_{buf}$  are currents in the presence and in the absence of each analyte,  $k$  is the catalytic rate constant ( $\text{M}^{-1}\text{s}^{-1}$ ) for the analyte oxidation and  $t$  is the time in seconds. Figure 4.13 shows the linear relationship for the  $I_{cat}$  and  $I_{buf}$  vs  $t^{1/2}$  plots for different analyte concentrations obtained from the chronoamperometric curves. The slope of Figure 4.13 is equal to  $\pi k$ . The values of  $k$  for ASA, IBU and INDO obtained were  $1.655 \times 10^1 \text{ M}^{-1}\text{s}^{-1}$ ,  $1.42 \times 10^1 \text{ M}^{-1}\text{s}^{-1}$  and  $1.91 \text{ M}^{-1}\text{s}^{-1}$  respectively. The values of  $k$  obtained were comparable with those obtained in literature [9]. This showed that CoTAPhPcNPs/n-CNDs-GCE was the best electrode for fast detection of ASA, IBU and INDO. Figure 4.13 insert shows the plot of peak current against concentration. A linear relationship was observed from all the plots. The regression equations obtained were  $y = 0.052[\text{ASA}] \text{ mM}^{-1}\text{s}^{-1} + 2 \times 10^{-6}$ ,  $R^2 = 0.938$

$$y = 0.0446[\text{IBU}] \text{ mM}^{-1}\text{s}^{-1} + 5 \times 10^{-6}, R^2 = 0.992$$

$$y = 0.006[\text{INDO}] \text{ mM}^{-1}\text{s}^{-1} + 1 \times 10^{-8}, R^2 = 0.993$$

The different accumulation efficiency at different concentrations results in different slopes of the six calibration curve for each analyte. The detection limits (LOD) of ASA, IBU and INDO using chronoamperometry were very low and they are displayed in table 4.3 below together with the limit of quantification (LOQ). The prepared modified electrode has a wider linear range and a lower detection limit for ASA, IBU and INDO. Even more tantalizing, it was easy to fabricate the CoTAPhPcNPs/n-CNDs-GCE. Therefore, the CoTAPhPcNPs/n-CNDs-GCE possessed high sensitivity to ASA, IBU and INDO with excellent electrocatalytic performance.

Table 4.3: Summary of the chronoamperometry studies

Molecule	Electrode	LOD(M)	LOQ(M)	Catalytic Constant <sup>1)</sup> (M <sup>-1</sup> s <sup>-1</sup> )	Rate Reference
<b>ASA</b>	CoTAPhPcNPs/n-CNDs-GCE.	7.7×10 <sup>-6</sup>	2.3×10 <sup>-5</sup>	1.655x 10 <sup>1</sup>	This work
<b>IBU</b>	CoTAPhPcNPs/n-CNDs-GCE.	3.6×10 <sup>-6</sup>	1.17×10 <sup>-5</sup>	1.42x 10 <sup>1</sup>	This work
<b>INDO</b>	CoTAPhPcNPs/n-CNDs-GCE.	7.24×10 <sup>-6</sup>	2.19×10 <sup>-5</sup>	1.91	This work
-	CoTAPhPcNPs-rBDGONS-GCE.	-	-	6.1x 10 <sup>1</sup>	[9]

#### 4.6.11 Determination of Limit of Detection

Differential pulse voltammetry has the advantage of an increase in sensitivity and better

characteristics for analytical application [45]. It is also a very sensitive technique for the analysis of trace concentrations of electro active species. The electrochemical response of ASA, IBU and INDO was carried out by employing DPV using CoTAPhPcNPs/n-CNDs-GCE in fig 4.14. The DPV parameters were evaluated in order to obtain the highest signal of ASA, IBU and INDO. A linear behavior with a good correlation coefficient was verified from 0.1  $\mu\text{M}$  to 0.6  $\mu\text{M}$ . The table below displays detection limit of each analyte compared to those in literature. The detection limit of ASA was found to be  $9.66 \times 10^{-7}$  and it was very low indicating that the CoTAPhPcNPs/n-CNDs-GCE has good catalytic performance. The detection limit of IBU and INDO were  $4.19 \times 10^{-7}$  and  $7.2 \times 10^{-7}$  respectively indicating that the feasibility of the proposed method was accurately determined. All the detection limits of all the analytes were very low and comparing the LODs with those in literature (table 4.4), CoTAPhPcNPs/n-CNDs-GCE was found to be a good sensor.

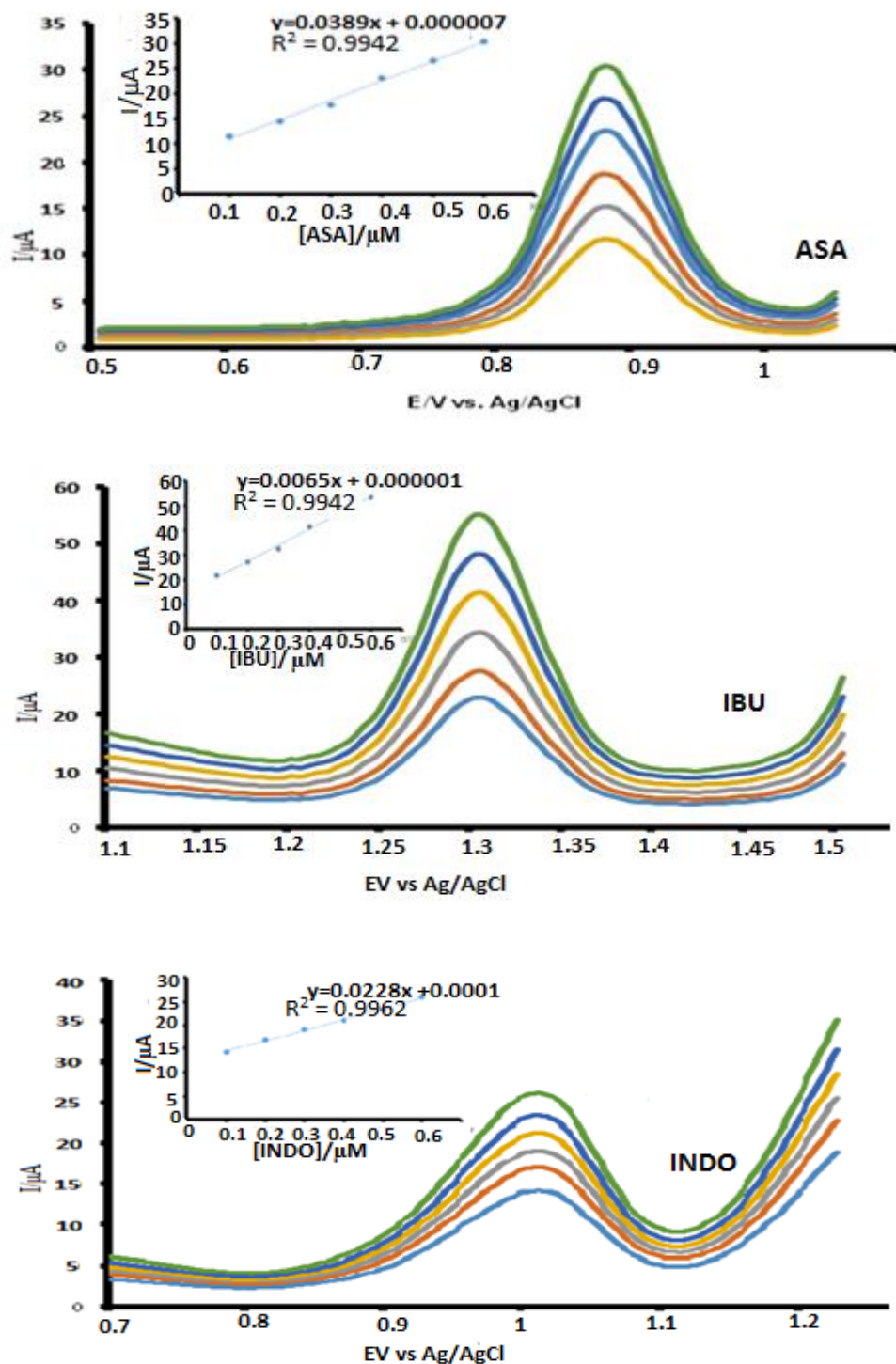


Fig 4.14: DPV for CoTAPhPcNPs/n-CNDs-GCE in: a) 0.1  $\mu\text{M}$ , b) 0.2  $\mu\text{M}$ , c) 0.3  $\mu\text{M}$ , d) 0.4  $\mu\text{M}$ , e) 0.5  $\mu\text{M}$ , f) 0.6  $\mu\text{M}$  ASA, IBU and INDO Inset: Plot of  $I_{pa}$  vs [ASA, IBU, and INDO]

Table 4.4: Detection limits of ASA, IBU and INDO

Analyte	Modifier	Linear working range(M)	Limit of Detection	Reference
<b>ASA</b>	BD GCE	$2.5 \times 10^{-6}$ - $1.05 \times 10^{-4}$	$2 \times 10^{-6}$	[46]
	Ni GCE	$2 \times 10^{-4}$ - $7 \times 10^{-3}$	$4.8 \times 10^{-5}$	[46]
	BD GCE	$1 \times 10^{-5}$ - $8 \times 10^{-5}$	$1.03 \times 10^{-6}$	[47]
	n-CNDs/CoTAPhPcNPs GCE	$1 \times 10^{-7}$ - $6 \times 10^{-7}$	$9.66 \times 10^{-7}$	This work
<b>IBU</b>	GCE	$3 \times 10^{-6}$ - $7 \times 10^{-4}$	$2 \times 10^{-6}$	[1]
	BD GCE	$2.5 \times 10^{-6}$ - $6 \times 10^{-4}$	$5 \times 10^{-6}$	[48]
	n-CNDs/CoTAPhPcNPs GCE	$1 \times 10^{-7}$ - $6 \times 10^{-7}$	$4.19 \times 10^{-7}$	This work
<b>INDO</b>	CPE	$1 \times 10^{-6}$ - $1.05 \times 10^{-3}$	$1 \times 10^{-5}$	[49]
	MWCNTs GCE	$1 \times 10^{-6}$ - $5 \times 10^{-5}$	$2.6 \times 10^{-6}$	[49]
	n-CNDs/CoTAPhPcNPs GCE	$1 \times 10^{-7}$ - $6 \times 10^{-7}$	$7.2 \times 10^{-7}$	This work

#### 4.6.12 Simultaneous differential pulse voltammetry studies

In order to test the feasibility of the proposed method for the determination[49] of IBU and INDO simultaneously, the relationship between the anodic peak current and the concentration of IBU and INDO was studied using DPV under the optimum conditions. Figure 4.15A shows the DPVs of IBU and INDO with increasing amounts of INDO at CoTAPhPcNPs/n-CNDs-GCE. The peaks of IBU are hardly changed throughout the test, which suggest that its oxidation product do not reversibly adsorb on the surface of CoTAPhPcNPs/n-CNDs-GCE to hinder the detection of INDO. The oxidation peak currents of INDO show a good linear relationship with

INDO concentrations. The limit of detection and limit of quantification were found to be  $1.02 \times 10^{-7}$  and  $3.65 \times 10^{-7}$  respectively. All these assays indicate that the proposed sensor allows simultaneous and sensitive detection of IBU and INDO without interference from each other. Furthermore, CoTAPhPcNPs/n-CNDs-GCE was applied for the simultaneous determination of IBU and INDO and there were increase in amounts of IBU as shown in Figure 4.15B. Two well-distinguished oxidation peaks are observed in Figure 4.15C, indicating that catalytic reactions of IBU and INDO at CoTAPhPcNPs/n-CNDs-GCE occur independently. Therefore, the results demonstrate that IBU and INDO can be selectively determined by, CoTAPhPcNPs/n-CNDs-GCE without interference from each other. This also demonstrates that the sensor holds great application prospect for simultaneous determination of pharmaceutical drugs. Therefore, in this study the DPV technique possesses higher sensitivity and better resolution than cyclic voltametry technique.

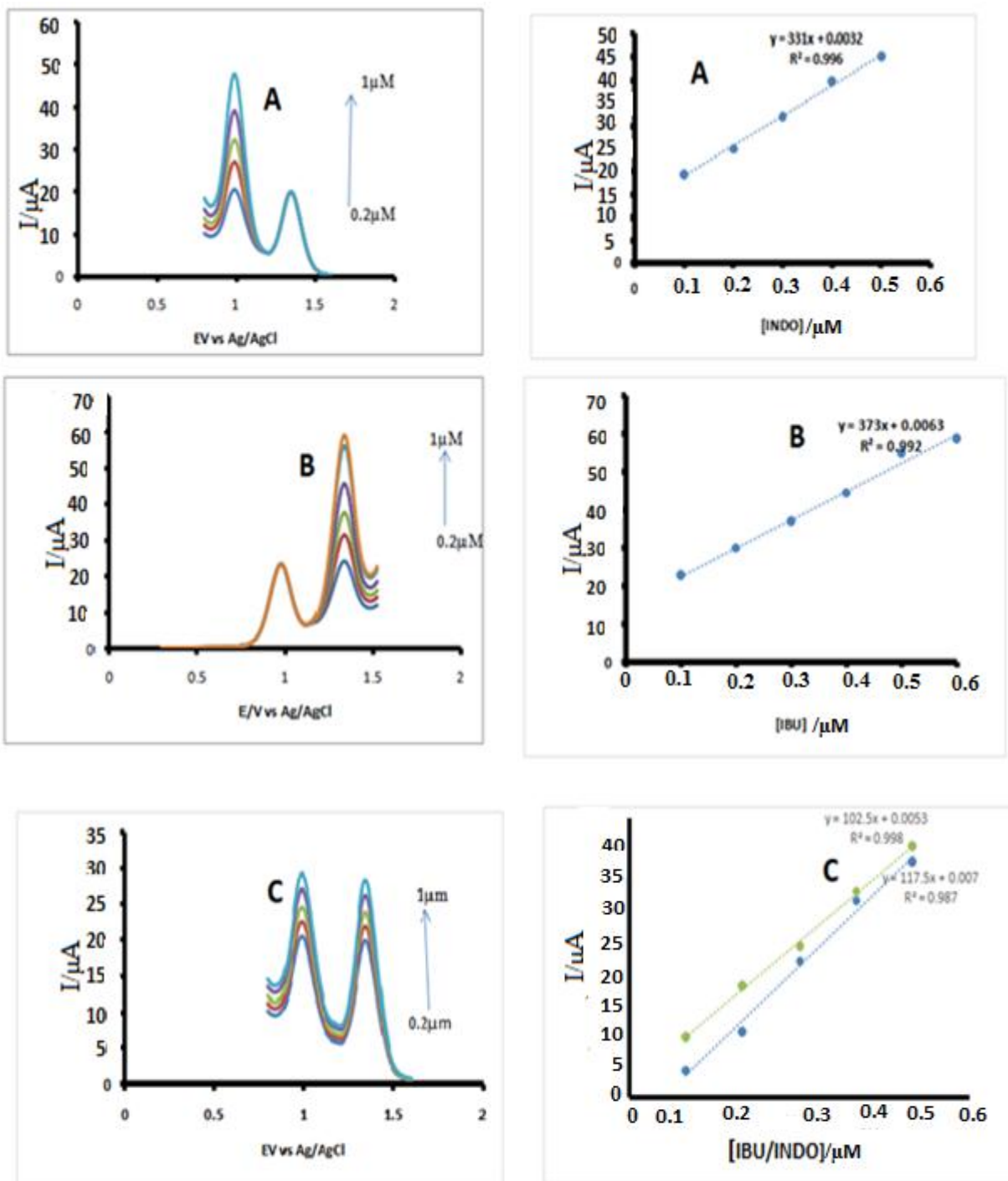


Fig 4.15: DPV for CoTAPhPcNPs/n-CNDs-GCE in PBS (pH 5.5) containing a mixture of A: 0.2-1.2 μM INDO, 0.2 μM IBU. B: 0.2-1.2 μM IBU, 0.2 μM INDO. Insets show the relationship of  $I_{pa}$  versus the concentrations of each analyte.

#### 4.6.13 Effect of concentration using impedimetric technique

Effect of concentration was also studied using Impedimetric technique in Figure 4.16A. In this work, IBU was used to study the effect of concentration. The results showed that as concentration increases, the semicircle decreases where the ionic/electronic charge transfer resistances show noticeable decrease in values indicating less electronic resistance and more conductivity. It can also be observed that both the charge transfer resistance and especially the interface resistance decreased when concentration of ibuprofen increased and there was accelerated electron transfer. The depressed arc radius of the Nyquist plot corresponds to the electron transfer limited process. There was a linear behaviour (Figure 4.16B) with a good correlation coefficient and  $R^2$  value was found to be 0.991. The technique was also used to determine limit of detection of IBU and it was found to be  $2.72 \times 10^{-7}$ . Therefore, Impedimetric technique is a very effective technique since it shows higher sensitivity for the detection of IBU.

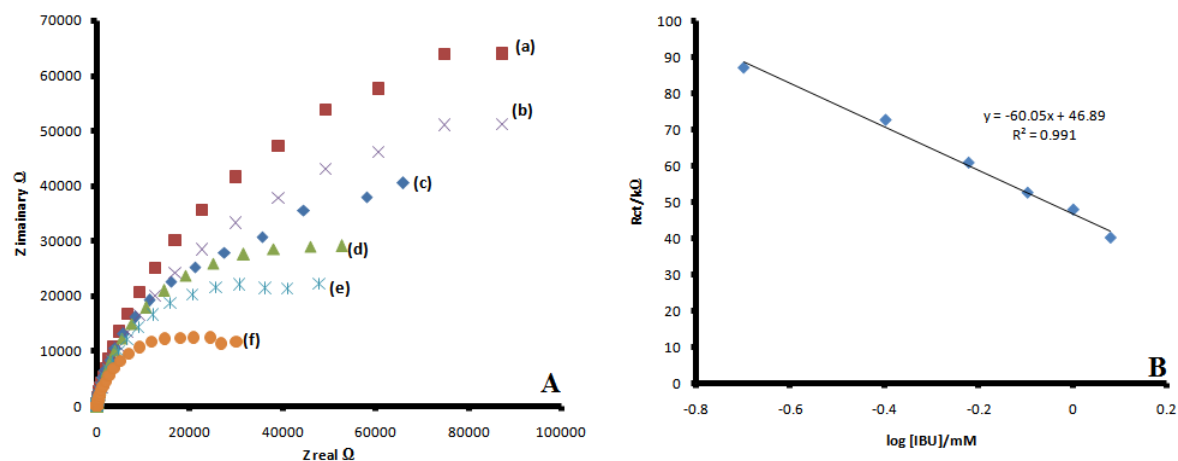


Fig 4.16: Complex plane impedance spectra at CoTAPhPcNPs/n-CNDs-GCE for different concentrations of IBU in pH 5 PBS and variation of Rct with log [IBU]

#### 4.6.14 Stability studies

The stability of CoTAPhPcNPs/n-CNDs-GCE towards oxidation of ASA, IBU and INDO was

checked by repetitive scanning (20 scans) in Figure 4.17. The results showed that the modified electrode has a good stability in aqueous solution after repeated cyclic voltammograms of modified electrode in 1mM ASA and 1mM IBU. In 1mM INDO, the anodic peak current decreases slightly and it was found that the shape of the voltammograms did not change. The signal loss in INDO was found to be 33%. Therefore, the good stability was indicated in ASA and IBU of the presented sensor.

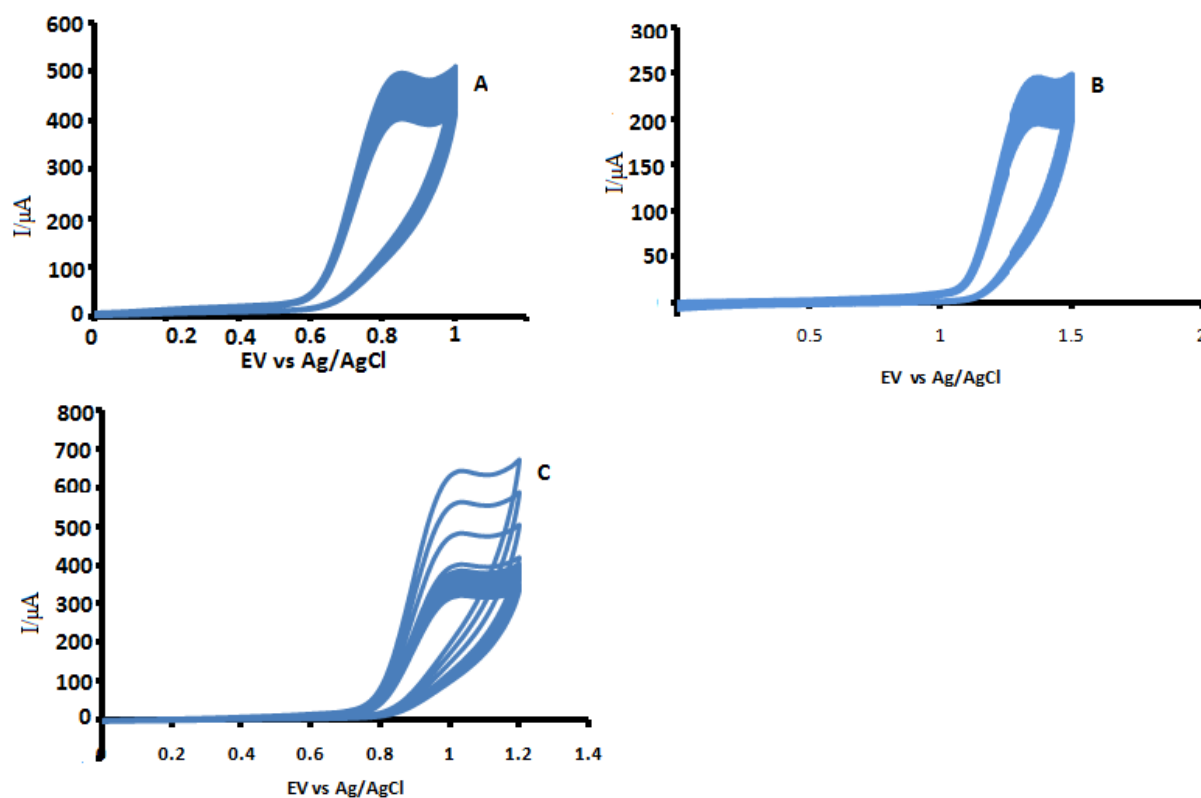


Fig 4.17: Continuous cyclic voltammetric evolutions for (A) ASA, (B) IBU and (C) INDO in PBS at CoTAPhPcNPs/n-CNDs-GCE. Scan rate = 100 mV/s

#### 4.6.15 Reproducibility studies

The sensitivity of an electrochemical method should be accompanied by good reproducibility since reproducibility is a desirable feature for a sensor [50]. The modified electrode was rinsed

and sonicated for 30 minutes. In this study, reproducibility was checked by employing cyclic voltammetry technique (Figure 4.18). This was done for five times and cyclic voltammograms were recorded for ASA, IBU and INDO. Results obtained were compared with the CVs obtained in the same solutions. The signal loss for ASA, IBU and INDO was found to be 5.5%, 8.4% and 7.2% respectively. The results of each analyte showed that peak current decreased slightly revealing excellent reproducibility of the electrode preparation procedure.

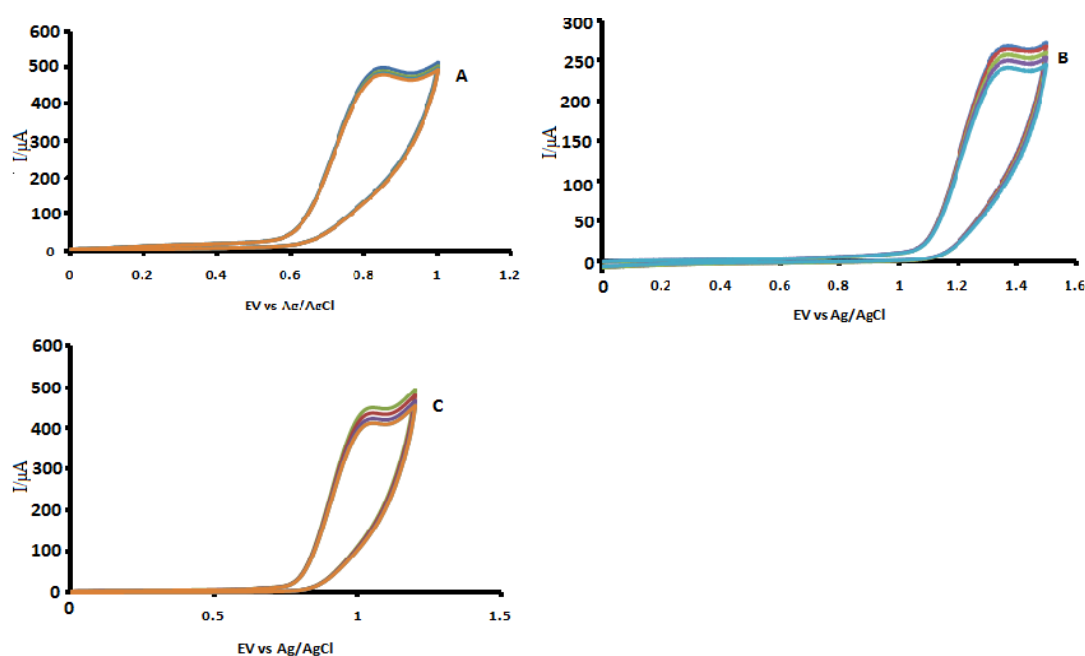


Fig 4.18: Cyclic voltammograms of (A) ASA, (B) IBU and (C) INDO in PBS at CoTAPhPcNPs/n-CNDs-GCE.

#### 4.6.16 Applicability

Applicability of developed sensor was evaluated by employing DPV for each analyte (Figure 4.19). Real-time monitoring performance of the fabricated sensor was checked by detecting ASA, IBU and INDO in real environmental water samples. The recoveries in table 4.6

are in the range of 90.6-101.8%, suggesting good feasibility and reliability of the proposed electrode for detection of ASA, IBU and INDO in waste water samples.

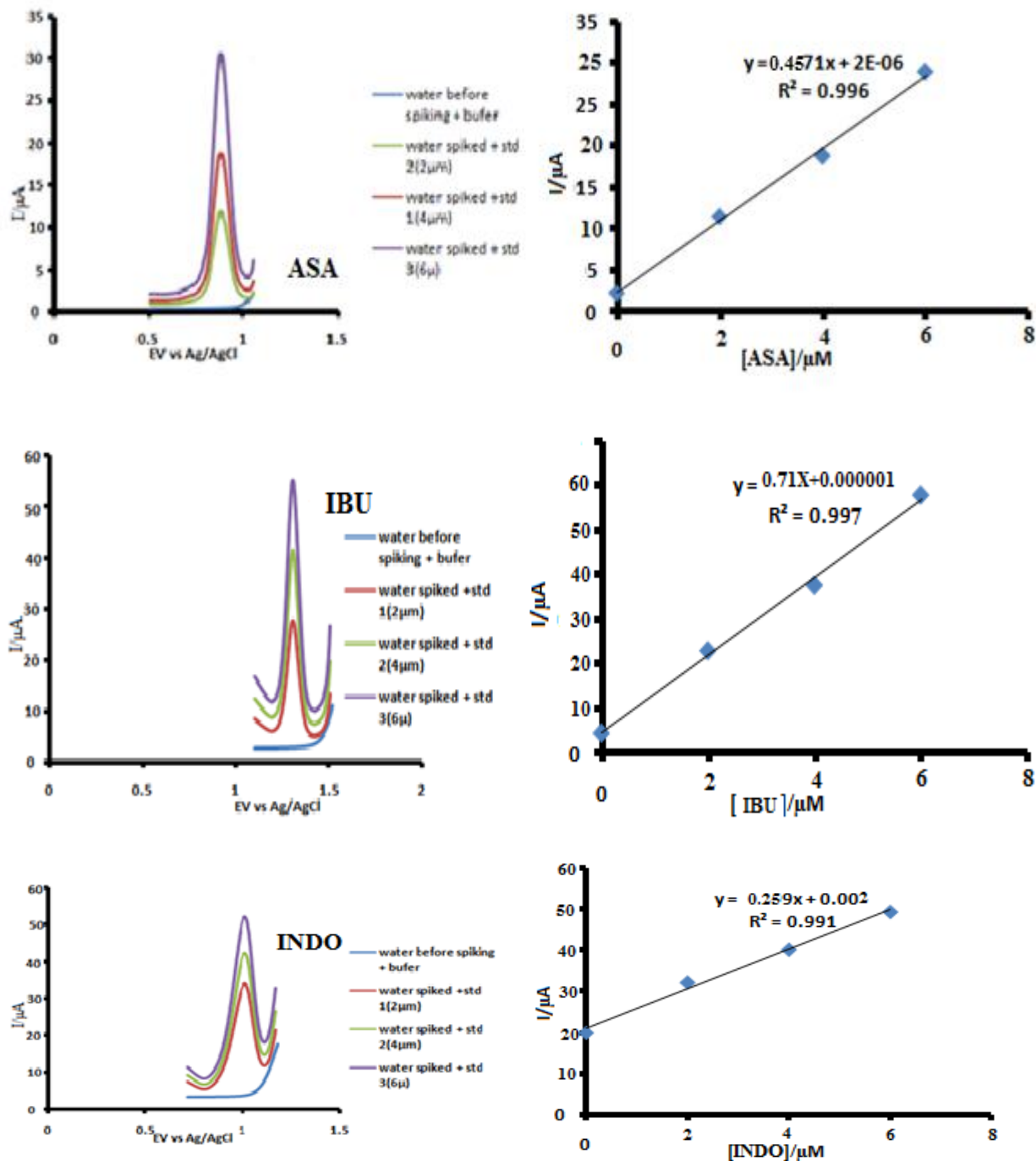


Fig 4.19: DPVs of the real sample analysis for each analyte

Table 4.5: Determination of drugs in waste water effluent using CoTAPhPcNPs/n-CNDs-GCE

Sample	Analyte	Added ( $\mu\text{M}$ )	Found ( $\mu\text{M}$ )	Recovery (%)
Waste water	ASA	0	$2.011 \times 10^{-6}$	-
		$2 \times 10^{-6}$	$2.033 \times 10^{-6}$	101.5
		$4 \times 10^{-6}$	$4.071 \times 10^{-6}$	101.8
		$6 \times 10^{-6}$	$6.025 \times 10^{-6}$	100.4
Waste water	IBU	0	$1.037 \times 10^{-6}$	-
		$2 \times 10^{-6}$	$1.926 \times 10^{-6}$	96.3
		$4 \times 10^{-6}$	$3.743 \times 10^{-6}$	93.6
		$6 \times 10^{-6}$	$5.471 \times 10^{-6}$	91.2
Waste water	INDO	0	$1.492 \times 10^{-6}$	-
		$2 \times 10^{-6}$	$1.894 \times 10^{-6}$	94.7
		$4 \times 10^{-6}$	$3.751 \times 10^{-6}$	93.8
		$6 \times 10^{-6}$	$5.437 \times 10^{-6}$	90.6

#### 4.6.17 Interference studies

One important aspect for the feasibility of a sensor is its capability to differentiate the analytes from interferences. In this work, the electrochemical responses of each analyte were measured at CoTAPhPcNPs/n-CNDs-GCE in the presence of different interferents (Figure 4.20). The effect of these species was determined using DPV and it was observed that there was no great significant change in the peak currents and peak potentials of the interfered species. The relative percentage response of the sensor calculated using the formulae:

$$(R \%) = \left[ 1 - \left( \frac{i^{\text{analyte}} + i^{\text{inter}}}{i^{\text{inter}}} \right) \right] \times 100 \quad (4.7)$$

where  $I^{\text{analyte}}$  and  $I^{\text{inter}}$  are the peak currents for an analyte and for the interfering respectively. The RSD % above 10 % shows that the compound interferes with the analyte. All the interferences showed that they have no effect as they had interference effect of less than 10 %. All these results suggest that the sensor has a satisfactory anti-interference ability for determination of ASA, IBU and INDO.

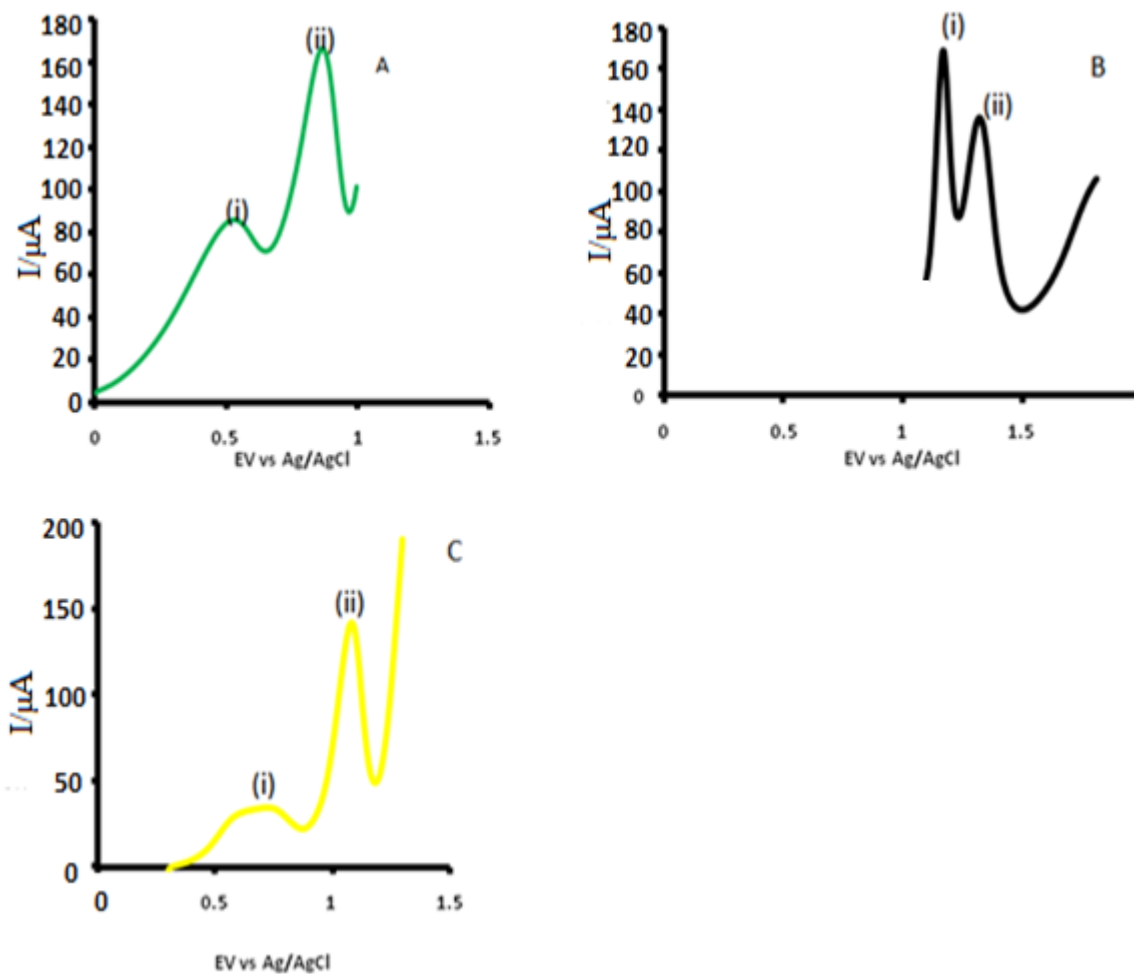


Fig 4.20: DPVs for (A) (i) ascorbic acid and (ii) ASA (B) (i) citric acid and (ii) IBU and (C) (i) glucose and (ii) INDO in PBS at n-CNDs/CoTAPhPcNPs GCE

## CHAPTER FIVE

### 5.1 Conclusion

On the basis of good electrochemical activity, an ultra-sensitive reproducible, stable and real-time applicable modified electrode CoTAPhPcNPs/n-CNDs-GCE was developed for the determination of ASA, IBU and INDO. A simple, productive method was used to synthesize n-CNDs with honeycomb-like porous structure. The n-CNDs showed excellent stability compared to non doped CNDs. The CoTAPhPcNPs/n-CNDs were characterized by FTIR and impedance methods. The excellent electrochemical performance of the composite (mixture of n-CNDs and CoTAPhPcNPs) is attributed to the continuous honeycomb like network with ultra thin walls doped nitrogen which facilitates the uniform distribution and anchoring of CoTAPhPcNPs. Due to unique properties of CoTAPhPcNPs and n-CNDs, the sensor exhibited remarkable electrochemical activity towards the oxidation of AS, IBU and INDO and also resolved the overlapping anodic peak response of ASA, IBU and INDO into well defined peaks. The modified electrode gave superior detection limits of ASA, IBU and INDO and they were found to be  $9.66 \times 10^{-7}$ ,  $4.19 \times 10^{-7}$  and  $7.2 \times 10^{-7}$  respectively. The association of differential pulse voltammetric studies and Chronoamperometric studies with standard addition method has been used for a fast analytical evaluation of ASA, IBU and INDO. The developed sensor has excellent sensor performance towards detection of IBU and INDO simultaneously. Moreover, the proposed method was very sensitive free of common interferences. The studies revealed that CoTAPhPcNPs/n-CNDs have significantly improved sensor performance in comparison with other previously developed chemical modifiers. The assay demonstrated in ASA, IBU and INDO revealed the good practical feasibility of the CoTAPhPcNPs/n-CNDs-GCE in drug analysis.

## 5.2 Recommendations

In this study, the dip and dry method for electrode modification was used. The process involves the modifier solution being dropped onto the electrode surface and then allowed to dry. The advantage of this modification process is that it is fast and a relatively stable CoTAPhPcNPs/n-CNDs layer can be formed on carbon based electrodes where  $\pi$ - $\pi$  interactions can occur between the MPc and n-CNDs, and the substrate surface. The disadvantages are that the electrode surfaces are not reproducible and unstable over long periods of time. Further work can be done using different electrode modification techniques so as to promote excellent reproducibility.

The developed sensor failed to detect ASA by using the DPV technique. Further studies can be pursued using other metallophthalocyanines such as Ni or Fe as both metallophthalocyanines have been used in previous studies as electrode modifiers. Different morphologies of metallic nanoparticles have been produced by using different solvents. The morphology and particle size of metal nanoparticles may in addition be controlled by reaction temperature, the concentration of metal precursors and the type of reducing agent, and in turn these morphologies may have an effect on the electrochemical process. Thus further studies can be undertaken to observe the nanoparticles morphologies so as to observe the different sizes and shapes, and how they affect the electrochemical process. Carbon nanodots produced in this work are large and they are not in the required range of 10 nm. The CNDs should be produced in a free dust environment and other synthesis methods such as microwave synthesis should be done. Aspects in the research that can be improved include further conjugation of the overall n-CNDs and CoTAPhPcNPs.

## References

- [1] N. Suresh, E. Sundaram, B. Kavitha, S. Maria Rayappan, “simultaneous electrochemical determination of paracetamol and ibuprofen at the glassy carbon electrode,” *J. Adv. Chem. Sci.*, 2, 4, 369–372, **2016**.
- [2] S. R. Sataraddi, S. M. Patil, A. M. Bagoji, V. P. Pattar, and S. T. Nandibewoor, “Electrooxidation of Indomethacin at Multiwalled Carbon Nanotubes-Modified GCE and Its Determination in Pharmaceutical Dosage Form and Human Biological Fluids,” *Anal. Chem.*, 1–9, **2014**.
- [3] Y. M. Issa, S. I. M. Zayed, and I. H. I. Habib, “Simultaneous determination of ibuprofen and paracetamol using derivatives of the ratio spectra method,” *Arab. J. Chem.*, 4, 3, 259–263, **2011**.
- [4] R. Hamoudová and M. Pospíšilová, “Determination of ibuprofen and flurbiprofen in pharmaceuticals by capillary zone electrophoresis,” *J. Pharm. Biomed. Anal.*, 41, 4, 1463–1467, **2006**.
- [5] S. Motoc, “Electrochemical selective and simultaneous detection of diclofenac and ibuprofen in aqueous solution using hkust-1 metal-organic framework-carbon nanofiber composite electrode,” *Sensors (Switzerland)*, 16, 1–10, **2016**.
- [6] M. O. Iwunze, “Absorptiometric determination of acetylsalicylic acid in aqueous ethanolic solution,” *Anal. Lett.*, 41, 16, 2944–2953, **2008**.
- [7] P. Manjunatha, C. C. Vidyasagar, and Y. A. Nayaka, “Voltammetric Studies of Aspirin in Pharmaceutical Sample Using Ctab - Pencil Graphite Electrode,” *Org. Med. Chem.*, 1, 3, 1–5, **2017**.
- [8] B. O. Agboola, A. Mocheke, J. Pillay, and K. I. Ozoemena, “Nanostructured cobalt phthalocyanine single-walled carbon nanotube platform: electron transport and

- electrocatalytic activity on epinephrine,” *J. Porphyr. Phthalocyanines*, 12, 12, 1289–1299, **2008**.
- [9] M. Shumba and T. Nyokong, “Electrode modification using nanocomposites of boron or nitrogen doped graphene oxide and cobalt (II) tetra aminophenoxy phthalocyanine nanoparticles,” *Electrochim. Acta*, 196, 457–469, **2016**.
- [10] M. C. Ortega-liebana, “Uniform luminescent carbon nanodots prepared by rapid pyrolysis of organic precursors confined within nanoporous templating structures,” *Carbon N. Y.*, 117, 2017, 437–446, **2017**.
- [11] H. Li, Z. Kang, Y. Liu, and S.-T. Lee, “Carbon nanodots: synthesis, properties and applications,” *J. Mater. Chem.*, 22, 46, 24220–24230, **2012**.
- [12] H. Zheng, P. Niu, and Z. Zhao, “Carbon quantum dot sensitized Pt@Bi<sub>2</sub>WO<sub>6</sub>/FTO electrodes for enhanced photoelectro-catalytic activity of methanol oxidation,” *RSC Adv.*, 7, 43, 26943–26951, **2017**.
- [13] J. W. J. Margraf, F. Lodermeier, V. Strauss, P. Haines, “Nanoscale Horizons,” *Communication*, 1–7, **2016**.
- [14] Z. Xu, J. Lan, J. Jin, P. Dong, F. Jiang, and Y. Liu, “Highly Photoluminescent Nitrogen-Doped Carbon Nanodots and Their Protective Effects against Oxidative Stress on Cells Highly Photoluminescent Nitrogen-Doped Carbon Nanodots and Their Protective Effects against Oxidative Stress on Cells,” *Appl. Mater. Interfaces*, 1–26, **2015**.
- [15] B. Shi, Y. Su, L. Zhang, M. Huang, R. Liu, and S. Zhao, “Nitrogen and Phosphorus Co-doped Carbon Nanodots as a Novel Fluorescent Probe for Highly Sensitive Detection of Fe<sup>3+</sup> in Human Serum and Living Cells Nitrogen and Phosphorus Co-doped Carbon Nanodots as a Novel Fluorescent Probe for Highly Sensitive Detect,” *Appl. Mater.*

- Interfaces*, 1–33, **2016**.
- [16] V. Strauss, “Assigning Electronic States in Carbon Nanodots,” *Adv. Funct. Mater.*, 1–11, **2016**.
- [17] S. Do, W. Kwon, and S.-W. Rhee, “Soft-template synthesis of nitrogen-doped carbon nanodots: tunable visible-light photoluminescence and phosphor-based light-emitting diodes,” *J. Mater. Chem. C*, 2, 21, 4221, **2014**.
- [18] X. G. and Y. W. Niu Jingjing, Hui Gao, Litao Wng, Shuangyu Xin, Gang Zhang, Qian Wang, Linna Guo, “Facile synthesis and optical properties of nitrogen-doped carbon dots †,” *R. Soc. Chem.*, 38, 1522–1527, **2014**.
- [19] S. Arslan, “Phthalocyanines : Structure , Synthesis , Purification and Applications,” *Life Sci.*, 6, 2, 188–197, **2016**.
- [20] S. Chohan, I. N. Booyesen, and A. Mambanda, “Synthesis , characterization and electrocatalytic behavior of cobalt and iron phthalocyanines bearing chromone or coumarin substituents,” *Coord. Chem.*, 1–20, **2015**.
- [21] S. Stepanow, “Spin Tuning of Electron-Doped Metal – Phthalocyanine Layers,” *J. Am. Chem. Soc.*, 136, 5451–5459, **2014**.
- [22] A. B. Sorokin, “Phthalocyanine Metal Complexes in Catalysis,” *Chem. Rev.*, 1–40, **2013**.
- [23] P. Reddyprasad, B. Naidoo, and N. Y. Sreedhar, “Electrochemical preparation of a novel type of C-dots/ZrO<sub>2</sub> nanocomposite onto glassy carbon electrode for detection of organophosphorus pesticide,” *Arab. J. Chem.*, 1–10, **2015**.
- [24] H. Zhang, S. Kang, G. Wang, Y. Zhang, and H. Zhao, “Fluorescence Determination of Nitrite in Water Using Prawn-Shell Derived Nitrogen-Doped Carbon Nanodots as Fluorophores,” *ACS Sensors*, 1, 7, 875–881, **2016**.

- [25] J. Li, “Nitrogen-doped carbon dots as a fluorescent probe for the highly sensitive detection of  $\text{Ag}^+$  and cell imaging,” *Luminescence*, 1–6, **2017**.
- [26] H. Wang, Q. Lu, Y. Liu, H. Li, Y. Zhang, and S. Yao, “A dual-signal readout sensor for highly sensitive detection of iodide ions in urine based on catalase-like reaction of iodide ions and N-doped C-dots,” *Sensors Actuators, B Chem.*, 250, 429–435, **2017**.
- [27] L. He, H. Zhang, H. Fan, X. Jiang, W. Zhao, and G. Q. Xiang, “Carbon-dot-based dual-emission silica nanoparticles as a ratiometric fluorescent probe for vanadium(V) detection in mineral water samples,” *Spectrochim. Acta - Part A Mol. Biomol. Spectrosc.*, 189, 51–56, **2018**.
- [28] N. Karikalan, R. Karthik, S.-M. Chen, and H.-A. Chen, “A voltammetric determination of caffeic acid in red wines based on the nitrogen doped carbon modified glassy carbon electrode,” *Sci. Rep.*, 7, 1, 45920-45924, **2017**.
- [29] J.-Y. Huang, T. Bao, T.-X. Hu, W. Wen, X.-H. Zhang, and S.-F. Wang, “Voltammetric determination of levofloxacin using a glassy carbon electrode modified with poly(o-aminophenol) and graphene quantum dots,” *Microchim. Acta*, 184, 1, 127–135, **2017**.
- [30] S. C. Tan, S. F. Chin, and S. C. Pang, “Disposable carbon dots modified screen printed carbon electrode electrochemical sensor strip for selective detection of ferric ions,” *J. Sensors*, 2017, 1–8, **2017**.
- [31] H. Wang, “Multifunctional  $\text{TiO}_2$  nanowires-modified nanoparticles bilayer film for 3D dye-sensitized solar cells,” *Optoelectron. Adv. Mater. Rapid Commun.*, 4, 8, 1166–1169, **2010**.
- [32] Z. Sheng, L. Shao, J. Chen, W. Bao, F. Wang, and X. Xia, “Catalyst-Free Synthesis of Nitrogen-Doped Graphene via Thermal Annealing Graphite Oxide with Melamine and Its

- Excellent Electrocatalysis,” *ACS Nano*, 5, 6, 4350–4358, **2011**.
- [33] B. D. B. and A. M. Mukherjee Anwasha, Siva K, “Influence of charge traps in carbon nanodots on gas interaction,” *IOP Sci.*, 1–16, **2017**.
- [34] P. Mashazi, J. Limson, and T. Nyokong, “Applications of polymerized metal tetra-amino phthalocyanines towards hydrogen peroxide detection,” *J. Porphyr. Phthalocyanines*, 14, 252–263, **2010**.
- [35] V. Gude, “Synthesis of hydrophobic photoluminescent carbon nanodots by using L-tyrosine and citric acid through a thermal oxidation route,” *Beilstein J. Nanotechnol.*, 5, 1, 1513–1522, **2014**.
- [36] N. Pandey, R. K. Srivastava, M. Kumar Singh, and J. Singh, “Optical properties of carbon nanodots synthesized by laser induced fragmentation of graphite powder suspended in water,” *Mater. Sci. Semicond. Process.*, 27, 1, 150–153, **2014**.
- [37] G.-A. Du Bao-Shan, “A simple and sensitive electrochemical detection of furazolidine based on Au nanoparticles functionalized graphene modified electrode,” *R. Soc. Chem.*, 1–20, **2017**.
- [38] S. Yang, “Simple synthesis of ZnO nanoparticles on N-doped reduced graphene oxide for the electrocatalytic sensing of L -cysteine,” *RSC Adv.*, 7, 35004–35011, **2017**.
- [39] O. E. Fayemi, A. S. Adekunle, and E. E. Ebenso, “Biosensors & Bioelectronics Metal Oxide Nanoparticles / Multi-walled Carbon Nanotube Nanocomposite Modified Electrode for the Detection of Dopamine: Comparative Electrochemical Study,” *Biosens. Bioelectron.*, 6, 4, 1–14, **2015**.
- [40] T. N. Philani Mshazi, Tawanda Mugadza, Ndabenhle Sosibe, Phumlubi Mdluli, Sibulelo Vilakazi, “Talanta The effects of carbon nanotubes on the electrocatalysis of hydrogen

- peroxide by,” *Electrochim. Acta*, 85, 2011, 2202–2211, **2011**.
- [41] S. Azab and A. M. Fekry, “Electrochemical design of a new nanosensor based on cobalt nanoparticles, chitosan and MWCNT for the determination of daclatasvir: a hepatitis C antiviral drug,” *RSC Adv.*, 7, 2, 1118–1126, **2017**.
- [42] L. Fu, G. Lai, and A. Yu, “Preparation of  $\beta$ -cyclodextrin functionalized reduced graphene oxide: application for electrochemical determination of paracetamol,” *RSC Adv.*, 5, 94, 76973–76978, **2015**.
- [43] S. A. Bhat, “Self-assembled AuNPs on sulphur-doped graphene: a dual and highly efficient electrochemical sensor for nitrite ( $\text{NO}_2^-$ ) and nitric oxide (NO),” *R. Soc. Chem.*, 41, 16, 1–14, **2017**.
- [44] P. L. Cheng Dan, Xi Li, Yan Qiu, Qi Chen, Jian Zhou, Yuqin Yang, Zhizhong Xie, “A simple modified electrode based on MIL-53 Fe for highly sensitive detection of hydrogen peroxide and nitrite,” *R. Soc. Chem.*, 1–15, **2017**.
- [45] F. G. N. S. S. Hadi Beitollahi, “GO/Fe<sub>3</sub>O<sub>4</sub>@SiO<sub>2</sub> core-shell nanocomposite modified graphite screen-printed electrode for sensitive and selective electrochemical sensing of dopamine and uric acid,” *R. Soc. Chem.*, 1–26, **2017**.
- [46] B. J. Sanghavi and A. K. Srivastava, “Electrochimica Acta Simultaneous voltammetric determination of acetaminophen, aspirin and caffeine using an in situ surfactant-modified multiwalled carbon nanotube paste electrode,” *Electrochim. Acta*, 55, 28, 8638–8648, **2010**.
- [47] C. Cofan and C. Radovan, “Anodic Determination of Acetylsalicylic Acid at a Mildly Oxidized Boron-Doped Diamond Electrode in Sodium Sulphate Medium,” *Int. J. Electrochem.*, 1–9, **2011**.

- [48] A. B. Lima, "Electrochemical Oxidation of Ibuprofen and Its Voltammetric Determination at a Boron-Doped Diamond Electrode," *Electroanalysis*, 25, 7, 1585–1588, **2013**.
- [49] M. J. Kianoush Sarhangzadeh, Habib Razmi, Rahim Mohammad-Rezaei, "Carbon Nanotube Composite Modified Carbon-Ceramic," *Anal. Lett.*, 1–27, **2014**.
- [50] H. N. Kamyabi Ali Mohammad, "Templated Electrodeposition of vertically aligned copper oxide nanowire arrays on 3D Ni Foam Substrates for Determination of Glucosamine in Pharmaceutical Caplet Samples," *R. Soc. Chem.*, 1–22, **2017**.

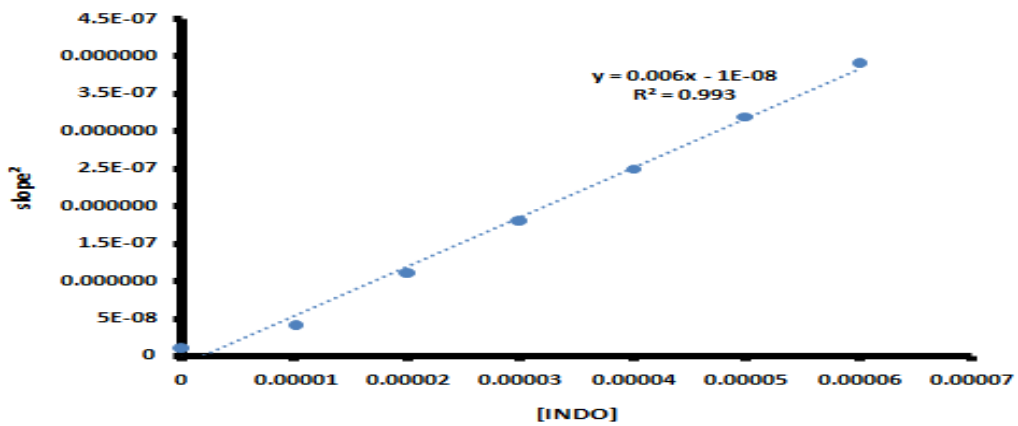
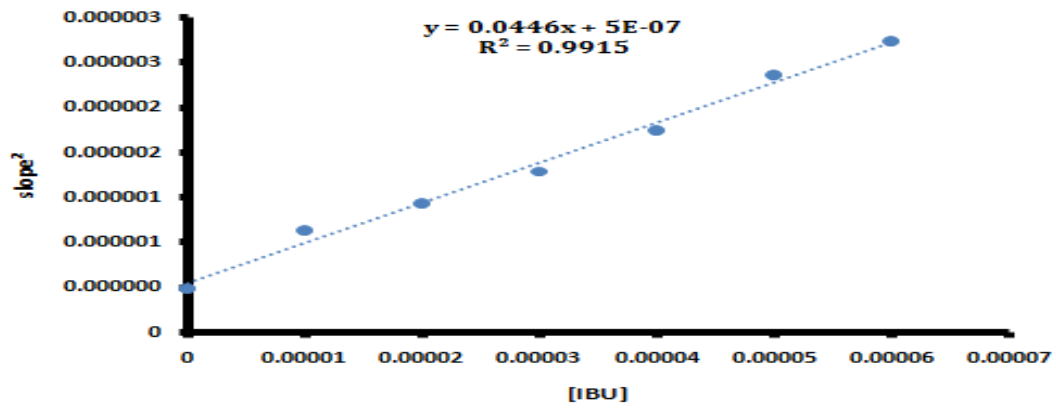
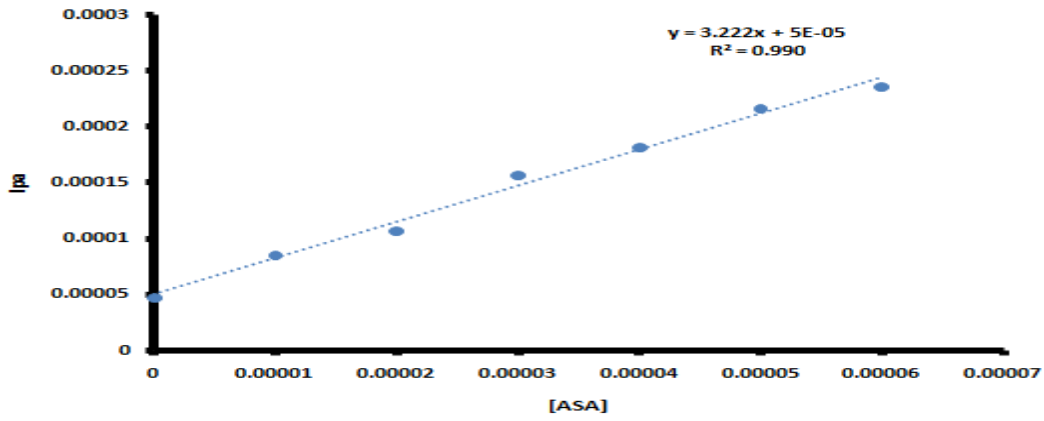
## APPENDIX

Table A.1: Instrumentation

<b>Name</b>	<b>Model</b>	<b>Manufacturer</b>	<b>Use</b>
Analytical Balance	GA-110	OHAUS	Weighing
pH meter	Az-8601	OHAUS	pH measurement
PGSTAT	PGSTAT302F	Autolab	Electrocatalysis
Ultra-Sonicator	KQ-250B	China Corp	Ultra agitation

### **Treatment of Glassware**

Laboratory liquid soap was used for washing all glassware and they were rinsed using distilled water to remove contaminants and impurities.



Chronoamperometry: Plot of  $slope^2$  vs [analyte]